Climate
of the Past
Discussions

No detectable influence of the carbonate ion effect on changes in stable carbon isotope ratios (δ^{13}C) of shallow dwelling planktic foraminifera over the past 160 kyr

Peter Köhler[1] and Stefan Mulitza[2]

[1]Alfred-Wegener-Institut Helmholtz-Zentrum für Polar-und Meeresforschung (AWI), Bremerhaven, Germany
[2]MARUM — Center for Marine Environmental Sciences and Faculty of Geosciences, University of Bremen, Germany

Correspondence: Peter Köhler (peter.koehler@awi.de)

Abstract. Laboratory experiments showed that the isotopic fractionation of δ^{13}C and of δ^{18}O during calcite formation of planktic foraminifera are species-specific functions of oceanic CO_3^{2-}-concentration. This effect became known as the carbonate ion effect (CIE), whose role during the interpretation of marine sediment data will be investigated here in an in-depth analysis of the ^{13}C cycle. For that effort we compiled new 160 kyr-long mono-specific stacks of changes in both δ^{13}C and δ^{18}O from

5   either the planktic foraminifera *G. ruber* (rub) or *T. sacculifer* (sac) from 112 and 40 non-polar marine records, respectively. Both mono-specific time series $\Delta(\delta^{13}C_{rub})$ and $\Delta(\delta^{13}C_{sac})$ are very similar to each other and a linear regression through a scatter plot of both data sets has a slope of $\sim$0.99 — although the laboratory-based CIE for both species differ by nearly a factor of two, implying that they should record distinctly different changes in δ^{13}C, if we accept that the carbonate ion concentration changes on glacial/interglacial timescales. For a deeper understanding we use the global carbon cycle model

10   BICYCLE-SE to calculate how surface ocean CO_3^{2-} should have varied over time in order to be able to calculate the potential corrections which would follow the laboratory-based CIE. Our simulations are forced with atmospheric reconstructions of CO_2 and $\delta^{13}CO_2$ derived from ice cores to obtain a carbon cycle which should at least at the surface ocean be as close as possible to expected conditions and which agrees in the deep ocean in the carbon isotope of dissolved inorganic carbon (DIC), $\delta^{13}C_{DIC}$, with reconstruction from benthic foraminifera. We find that both $\Delta(\delta^{13}C_{rub})$ and $\Delta(\delta^{13}C_{sac})$ agree better with changes in

15   simulated $\delta^{13}C_{DIC}$ when ignoring the CIE than those time series which where corrected for the CIE. The combination of data- and model-based evidence for the lack of a role for the CIE in $\Delta(\delta^{13}C_{rub})$ and $\Delta(\delta^{13}C_{sac})$ suggests to us that the CIE as measured in laboratory experiments is not directly transferable to the interpretation of marine sediments records. We hypothesise that both foraminifera species can optimise their light environments via vertical motion and therefore calcify under nearly stable CO_3^{2-} concentration. The much smaller CIE-to-glacial/interglacial-signal-ratio in δ^{18}O, when compared to δ^{13}C,

20   prevents us to draw robust conclusions on the role of the CIE on δ^{18}O as recorded in the hard shells of both species. However, theory proposes that the CIE in δ^{13}C and δ^{18}O depends both on the pH in the surrounding water, suggesting that the CIE should be detectable in neither or both of the isotopes. Whether this lack of role of the CIE in the interpretation of planktic paleo data

is a general feature, or restricted to the two species investigated here, needs to be checked with further data from other planktic foraminiferal species.

1 Introduction

The carbonate ion effect (CIE) describes that both δ^{13}C and δ^{18}O measured in hard shells of marine organisms undergo isotopic fractionation during calcite formation with the amplitude of the fractionation, among other factors, being a function of the carbonate ion concentration ($[CO_3^{2-}]$) of the surrounding seawater (Spero et al., 1997). The CIE has been found to be species-specific (Spero et al., 1999), ranging from -4.7 to -13.0×10^{-3} ‰ per μmol kg^{-1} of $[CO_3^{2-}]$ for δ^{13}C and between -1.4 and -4.5×10^{-3} ‰ per μmol kg^{-1} of $[CO_3^{2-}]$ for δ^{18}O in four planktic foraminifera. The CIE for δ^{13}C has been explained for *O. universa*, a spinose, symbiont bearing species, by the pH-related distribution of dissolved inorganic carbon (DIC) into its three species CO_2, CO_3^{2-}, and HCO_3^- (Wolf-Gladrow et al., 1999; Zeebe et al., 1999). The CIE on δ^{18}O is also explained by the CO_3^{2-}-related varying pH (Zeebe, 1999). The CIE is maybe the most prominent isotopic fractionation effect which asks for consideration when interpreting the paleo records, but others, e.g vital effects and dependency on light, temperature, pressure and shell size, have been put forward (e.g. Spero and Williams, 1988, 1989; Spero et al., 1991; Spero, 1992; Spero and Lea, 1993; Oppo and Fairbanks, 1989). The CIE is found to play a minor role when comparing late Holocene deep ocean δ^{13}C in benthic foraminifera with δ^{13}C of DIC ($\delta^{13}C_{DIC}$) (Schmittner et al., 2017) being responsible for -2.4×10^{-3} ‰ per μmol kg^{-1} of $[CO_3^{2-}]$ disturbance in the recorded signal. In a recent study focusing on the benthic species *C. wuellerstorfi* -3.0×10^{-3} ‰ per μmol kg^{-1} of $[CO_3^{2-}]$ have been obtained for the late Holocene (Nederbragt, 2023). Both studies also found in addition to the CIE that $\delta^{13}C_{benthic}$ was also partly controlled by other variables, mainly pressure (water depth) and temperature.

The CIE in planktic foraminifera is one of the reasons why the interpretation of the whole δ^{13}C cycle over glacial/interglacial timescales is still challenging. The data compilation of Oliver et al. (2010) covering the last 150 kyr of δ^{13}C in planktic and benthic foraminifera contained large uncertainties and did not consider potentially necessary corrections such as the CIE in the final interpretation. Since benthic compilations are less affected by the CIE, they should, however, robustly constrain deep ocean changes in $\delta^{13}C_{DIC}$. A more recent compilation of benthic δ^{13}C was given in Lisiecki (2014). Furthermore, δ^{13}C of atmospheric CO_2 ($\delta^{13}CO_2$) is now available over the last 155 kyr (Eggleston et al., 2016a) from ice cores. Missing in our understanding are so far tied constraints on change in surface ocean $\delta^{13}C_{DIC}$, but in principle these information should be recorded in the hard shells of planktic foraminifera, even if hidden under the CIE.

We therefore here aim to construct the first robust time series of orbital changes in surface ocean $\delta^{13}C_{DIC}$ based on planktic foraminifera data. We compile δ^{13}C data from the World Atlas of late Quaternary Foraminiferal Oxygen and Carbon Isotope Ratios (Mulitza et al., 2022) covering the last 160 kyr, in which data went through a rigorous quality control before entry and all applied age models have been revised to a most recent standard. In order to be able to apply any species-specific CIE corrections we compile mono-specific stacks using the widely abundant shallow-dwelling planktic foraminifera species *G. ruber* (rub) and *T. sacculifer* (sac). Due to their spatial distribution (Fraile et al., 2008) this species selection leads effectively
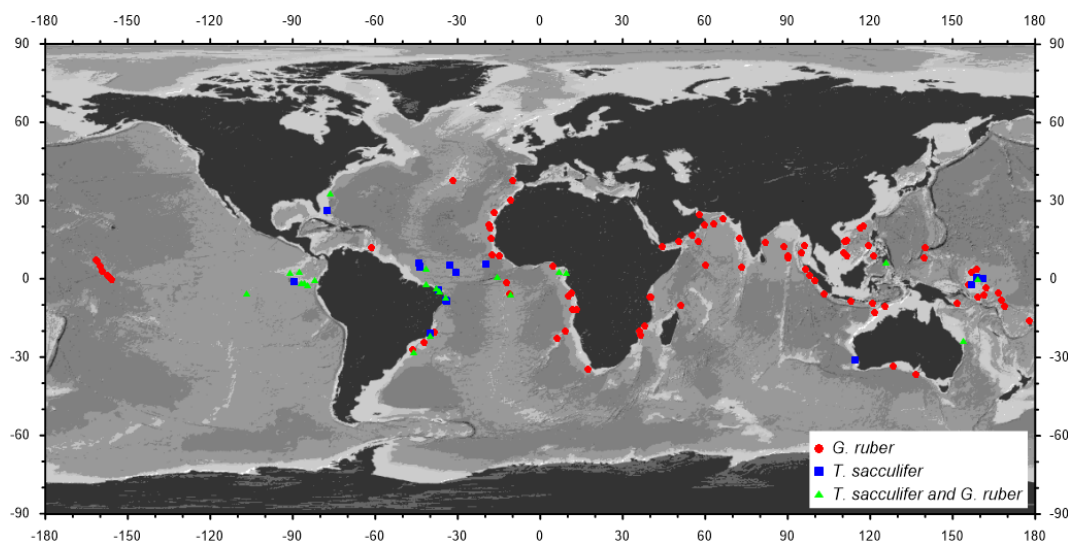
Figure 1. Location of the 127 sediment cores from which data have been compiled for this study. In 87 cores data from the planktic species *G. ruber* and in 18 cores data from *T. sacculifer* have been included, while 22 cores provided mono-specific data from both species.

to the construction of $\Delta(\delta^{13}C_{rub})$ and $\Delta(\delta^{13}C_{sac})$ stacks fed by sediment core data from the latitudes smaller than $40°$, potentially informing us about mean changes of $\delta^{13}C_{DIC}$ in the non-polar ocean on orbital timescales. Accompanied stacks of $\Delta(\delta^{18}O_{rub})$ and $\Delta(\delta^{18}O_{sac})$ from the same cores will add further information on the CIE in $\delta^{18}O$.

In the following we will investigate the connection of $\delta^{13}C$ in atmosphere and ocean in closer detail in order to improve our

60 understanding of the ^{13}C cycle. For this effort, we will first describe the construction of our mono-specific $\delta^{13}C$ anomaly stacks $\Delta(\delta^{13}C_{rub})$ and $\Delta(\delta^{13}C_{sac})$ (and of the accompanied $\delta^{18}O$ anomalies) and what we know about atmospheric $\delta^{13}CO_2$ and deep ocean $\delta^{13}C$ (section 2). Having two mono-specific stacks of surface ocean $\delta^{13}C$ enables us to address the CIE initially solely based on data. For a deeper interpretation the global isotope enabled carbon cycle model BICYCLE-SE (Köhler and Munhoven, 2020), which has been proven to simulate glacial/interglacial (G/IG) changes in the carbon cycle reasonably well,

65 is used. The parametrisation of the ^{13}C cycle in BICYCLE-SE is completely revised for this study (section 3). We then analyse $\delta^{13}C$ in our model simulations (section 4.1). This enables us to evaluate if our stacks $\Delta(\delta^{13}C_{rub})$ and $\Delta(\delta^{13}C_{sac})$ are good representations of changes in $\delta^{13}C_{DIC}$ in the non-polar surface ocean or if corrections such as the CIE need to be applied (section 4.2). Finally, we briefly discuss the CIE in $\delta^{18}O_{rub}$ and $\delta^{18}O_{sac}$ (section 4.3), before we come to our conclusions (section 5).
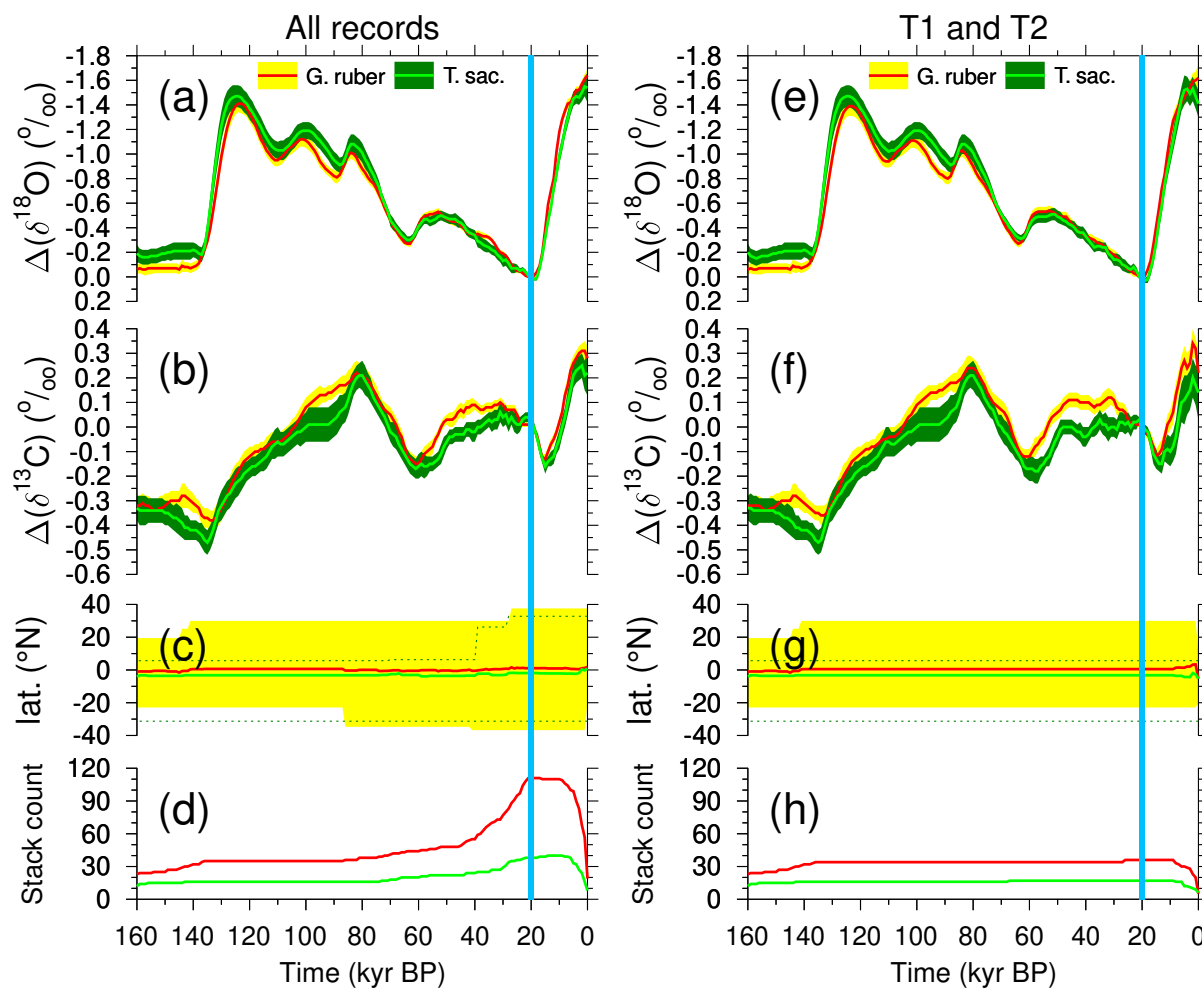
Figure 2. Stacks of anomalies in (a) $\delta^{18}O$ and (b) $\delta^{13}C$ from the planktic species *G. ruber* and *T. sacculifer* across the last 160 kyr. Mean anomalies (± 1 SE) are calculated with respect to the mean of 21–19 kyr BP (blue vertical band). Data are based on Mulitza et al. (2022). (c) Latitudinal distribution of cores contributing to the stack (mean and full range) and (d) stack count. Either data from all cores for each species are compiled (left) or (right) from a reduced core selection, in which contributing cores cover both Termination 1 and 2 (T1+T2).

2 Data on $\delta^{13}C$ changes

2.1 Constructing new mono-specific stacks from planktic foraminifera

Data source and age modelling: To construct time series of low-latitude $\delta^{13}C$ variations through the past 160 kyr, we selected 112 and 40 $\delta^{13}C$ records of the shallow-dwelling planktic foraminifera *G. ruber* and *T. sacculifer*, respectively, from the World Atlas of late Quaternary Foraminiferal Oxygen and Carbon Isotope Ratios (Mulitza et al., 2022). Since the publication of the 2022 version of the World Atlas various other records have been added to this repository. From these newly added records six

are actually containend in our data selection here. A list of the sediment cores from which data are contributing to our stacks with relevant meta data, references to the original publications and data sources is compiled in Table S1. In three sediment cores time series from both *G. ruber white* and *G. ruber pink* contribute to our *G. ruber* stacks, while data from 22 cores contain mono-specific data from both *G. ruber* and *T. sacculifer*. All combined our data selection is based on material from

80   127 sediment cores. The core sites cover a latitudinal range from 37.6°N to 36.7°S for *G. ruber* and of 32.8°N to 31.3°S for *T. sacculifer* in all major ocean basins (Figure 1), although the contributions from individual cores (and therefore the latitudinal range) changed over time (Figure 2c). Our age models are based on either radiocarbon ages or oxygen isotope stratigraphy or a combination of both methods. To calibrate radiocarbon ages, we first subtracted a simulated local reservoir age from the nearest grid-box of the modelling experiments conducted for Marine20 (Butzin et al., 2020; Heaton et al., 2020) and then calibrated

85   the corrected radiocarbon age with the IntCal20 calibration curve (Reimer et al., 2020). For core sections with insufficient radiocarbon coverage or outside the radiocarbon dating range ages were added through the visual alignment with the software PaleoDataView (Langner and Mulitza, 2019) using the isotope stacks by Lisiecki and Raymo (2005) and Lisiecki and Stern (2016). In an few cases age models were derived by visual alignment with the oxygen isotope records of well-dated nearby cores. The details of the age model construction are available in the netCDF files of the age models in the corresponding

90   PaleoDataView collection (Köhler and Mulitza, 2023). A continuous age model was then constructed with the age modelling software BACON (Blaauw and Christen, 2011). For each record we produced an ensemble of 1000 time series by combing 1000 BACON-generated age models with 1000 down-core δ^{13}C and δ^{18}O series by adding a random value within the typical analytical 1σ-uncertainty of 0.05% and 0.07‰ to each down-core δ^{13}C and δ^{18}O value, respectively. The resulting 1000 δ^{13}C and δ^{18}O time series were then interpolated to a time step of 1 kyr to calculate the mean and the standard deviation of the time

95   series ensembles. The averaging of the individual ensemble members then led to a considerable smoothing of the final time series.

Stacking of down-core isotope records: Sediment cores covering the Anthropocene clearly show that the δ^{13}C of *G. ruber* and *T. sacculifer* shells (δ^{13}C$_{rub}$, δ^{13}C$_{sac}$) faithfully reflects changes in δ^{13}C$_{DIC}$ (Al-Rousan et al., 2004; Black et al., 2011), albeit with a notable offset. This offset is influenced by the CIE (e.g. Spero et al., 1997), light intensity (e.g. Spero et al.,

100   1991) and the size of the foraminiferal shells (e.g. Oppo and Fairbanks, 1989). Although the size class used for stable isotope measurements can vary considerably among records, it is common practice to use a fairly constant size down-core to minimise size-related effects on both oxygen and carbon isotope ratios. To provide a common baseline, we corrected all single isotope records by their individual mean values for the period from 21 to 19 kyr BP marked as Last Glacial Maximum (LGM) in various plots. To produce final isotope stacks, we averaged all corrected time series and calculated the standard error (SE) of

105   the means at 1 kyr intervals. The final mono-specific stacks of both δ^{18}O and δ^{13}C anomalies based on either *G. ruber* or *T. sacculifer* are plotted in Figure 2a,b. The oxygen isotope stacks are here also shown to give a clear reference for G/IG changes, δ^{18}O has its maxima during peak glacial times and its minima during peak interglacials. In section 4.3 we will come back to these data to discuss the CIE in δ^{18}O$_{rub}$ and δ^{18}O$_{sac}$. We compiled two sets of data compilations, one to which all records contributed (Figure 2a–d), and another, in which only those records have compiled which covered both Terminations 1 and 2

110   (T1+T2, Figure 2e–h). The stack counts (Figure 2d,h) shows that the different compilations differ mainly in the younger half,

they are identical beyond 85 kyr BP. The latitudinal ranges in the young half are slightly smaller for the compilations T1+T2 than when all cores are compiled, but the mean latitudes of all cores are throughout the covered time window of the last 160 kyr in all cases (for both species and for both compilations) close to the equator (Figure 2d,g). This stationarity in the mean latitude suggests that the incoming light which varied in its annual mean values between $\sim$420 W m^{-2} at the equator and 115 $\sim$330 W m^{-2} around latitudes of 40° (Laskar et al., 2004) should only marginally affect the isotopic fractionation (e.g. Spero et al., 1991).

2.2 Benthic δ^{13}C

Focus of this study is the δ^{13}C of the surface ocean. However, for a rough comparison of δ^{13}C changes in the deep ocean we rely on the published δ^{13}C stack compiled from six deep Pacific core as contained in Lisiecki (2014). The six cores are all 120 ODP cores (677, 846, 849, 1123, 1143, 1208) from between 2700 and 3500 m water depth, located between 42°S and 36°N. The deep Pacific δ^{13}C stack should cover the most depleted end member of the marine δ^{13}C cycle (Figure 3d) and should give us some indication how δ^{13}C in deep ocean is performing in our simulations. More details on the stack are found in Lisiecki (2014).

2.3 Overview on ^{13}C cycle changes over the last 160 kyr

125 Reconstructed changes in the late Quaternary carbon cycle are still not completely understood. The ice cores give us a precise picture of atmospheric CO$_2$ (Bereiter et al., 2015; Köhler et al., 2017a) (Fig. 3a), which in the meantime has also been met reasonably well with various different carbon cycle models (e.g. Menviel et al., 2012; Ganopolski and Brovkin, 2017; Köhler and Munhoven, 2020). These findings suggest, that the main processes responsible for the observed changes on orbital timescales might indeed have been identified, although improvements in details are certainly necessary.

130 The corresponding atmospheric δ^{13}CO$_2$, now available over the last 155 kyr (Eggleston et al., 2016a), however, is in all its features still waiting for a process-based interpretation (Figure 3b). Since δ^{13}CO$_2$ helps to pinpoint on processes responsible for CO$_2$ changes, any simulation that is able to explain one without the other might need to be interpreted with caution. Models suggest that especially physical and biological processes in the Southern Ocean processes robustly influence δ^{13}CO$_2$, while the impact of the Atlantic meridional overturning circulation (AMOC) on δ^{13}CO$_2$ seems to be model-dependent (Menviel et al., 135 2015). Consequently, the abrupt drop in δ^{13}CO$_2$ at the onset of Termination 1 (T1) (Smith et al., 1999; Schmitt et al., 2012) is nowadays understood to be caused by marine processes, while subsequent δ^{13}CO$_2$ changes during T1 and its recovery during the Holocene to LGM-like values were potentially related to a mixture of oceanic and terrestrial processes (Köhler et al., 2005; Bauska et al., 2016).

Two surprising and largely unexplained features stand out in the 155 kyr δ^{13}CO$_2$ record. First, there exist a long-term trend 140 by +0.45‰ from the Penultimate and the Last Glacial Maximum (PGM and LGM). When first discovered (Schneider et al., 2013) it has been hypothesised that changes in the isotopic composition of solid Earth fluxes or of their intensities or long-term peat build-up might be responsible for them. Second, a 0.5‰ deep and nearly 20 kyr long minima centred around 58 kyr BP happened, rather uncorrelated with CO$_2$ changes. Eggleston et al. (2016a) hypothesise that the δ^{13}CO$_2$ minima might have been
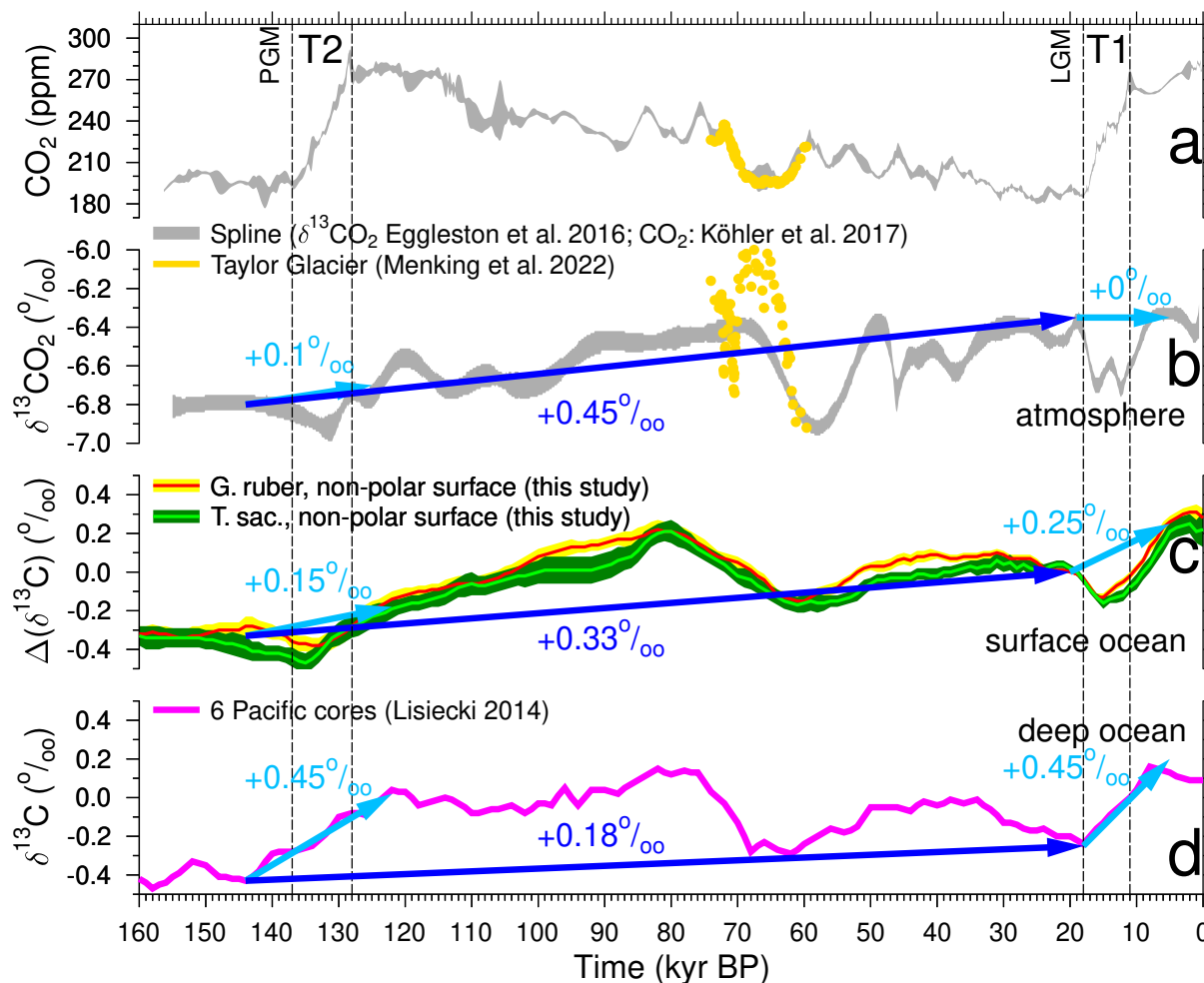
Figure 3. Carbon cycle time series of the last 160 kyr, including the Penultimate and Last Glacial Maximum (PGM, LGM) and Terminations 1 and 2 (T1, T2). Spline of atmospheric CO_2 (a) and $\delta^{13}CO_2$ (b) based on data from various ice cores (grey, $\pm 1\sigma$ around the mean, (Köhler et al., 2017a; Eggleston et al., 2016a)) and highly resolved recent data from the "horizontal ice core" approach in Taylor Glacier (yellow, (Menking et al., 2022b)). (c) $\Delta(\delta^{13}C_{rub})$ and $\Delta(\delta^{13}C_{sac})$ based on the planktic foraminifera *G. ruber* or *T. sac.*, respectively, averaging signals in the non-polar surface ocean (this study, based on Mulitza et al., 2022). (d) Deep ocean $\delta^{13}C$ from benthic foraminifera stacked from 6 Pacific cores (Lisiecki, 2014).

partially caused by a change in ocean stratification between Marine Isotope Stage (MIS) 4 and MIS 3, allowing for a different

145   amount of isotopically light carbon being stored in the deep ocean. Recently, high resolution data of $\delta^{13}CO_2$ from Taylor Glacier covering 74 to 59.5 kyr BP including MIS 4 and the drop into the $\delta^{13}CO_2$ minimum have been published (Menking et al., 2022b) showing more variability and between 66 and 60 kyr BP with $-1\%o$ a twice as large change as previously contained in the smoothed record of Eggleston et al. (2016a). Menking et al. (2022b) also performed first model simulations in order to

understand which processes might be responsible for the reconstructed changes in the carbon cycle. However, to our knowledge

150 none of the ideas put forward in Schneider et al. (2013) for the long-term trend in $\delta^{13}CO_2$ have so far been convincingly and successfully verified with carbon cycle model simulation. Furthermore, 400–500 kyr variability related to slow eccentricity changes found in marine Plio-Pleistocene $\delta^{13}C$ (Russon et al., 2010; Wang et al., 2014; Paillard, 2017) might be superimposed on faster variations, making a process-based understanding of observed changes in $\delta^{13}CO_2$ even more challenging.

Our new mono-specific stacks from the non-polar surface ocean of $\Delta(\delta^{13}C_{rub})$ and $\Delta(\delta^{13}C_{sac})$ without any corrections

155 (Figure 3c) contain a G/IG rise of 0.25‰ across T1, but of only 0.15‰ across T2, while atmospheric $\delta^{13}CO_2$ at the same time rose by 0.1‰ (T2), or stayed constant (T1) (Figure 3b), showing local minima during terminations in both records. Deep ocean benthic $\delta^{13}C$ (Figure 3d) is here approximated by a stack from six deep Pacific cores (Lisiecki, 2014), that contains a G/IG rise of 0.45‰ across both T1 and T2. This value is on the upper end of the 95% confidence interval of compilations of marine $\delta^{13}C$ changes across T1 (Peterson et al., 2014; Peterson and Lisiecki, 2018) which suggest to represent global ocean wide changes.

160 The marine time series, both from surface and deep ocean, also contain wide and deep minima around 60 kyr BP, similarly to the smoothed atmospheric $\delta^{13}CO_2$ data of Eggleston et al. (2016a), but different to the higher resolved Taylor Glacier $\delta^{13}CO_2$ of Menking et al. (2022b). Furthermore, all marine $\delta^{13}C$ data, similarly as the atmospheric $\delta^{13}CO_2$, contain a long-term rise from PGM to LGM (about +0.33‰ in the non-polar surface ocean, +0.18‰ in the deep Pacific, Figure 3) potentially connected with eccentricity related long-term variability of 400-to-500 kyr (Pälike et al., 2006; Ma et al., 2011; Wang et al., 2014), that

165 have been found in various parts of the Cenozoic.

Before we start with deeper model-based interpretation of the ^{13}C cycle, we have a closer look on our new isotope stacks. If the CIE plays a role for how the isotopes of the surface ocean are recorded in the foraminifera shells on orbital timescales then the two mono-specific time series in both $\delta^{13}C$ and $\delta^{18}O$ should differ, since the size of the CIE as detected from laboratory experiments in both species differs by nearly a factor of two, -0.0089 and -0.0047 ‰ change in $\delta^{13}C$ per μmol kg^{-1} of

170 $[CO_3^{2-}]$ for *G. ruber* and *T. sacculifer*, respectively, and of -0.0022 and -0.0014 ‰ change in $\delta^{18}O$ per μmol kg^{-1} of $[CO_3^{2-}]$ for *G. ruber* and *T. sacculifer*, respectively (Spero et al., 1999). At first glance (Figure 2a,b) the time series are remarkable similar. A more quantitative evaluation is obtained by calculating the linear regression from scatter plots, when results based on one species are plotted against those of the other. Doing so (Figure 4) reveals for $\delta^{13}C$ that on average changes are identically recorded in both species. In other words, the linear slope of $\Delta(\delta^{13}C_{rub})$ against $\Delta(\delta^{13}C_{sac})$ is 0.98 ($r^2 =$

175 0.95) or 0.99±0.03 ($r^2 = 0.95$) when considering the uncertainties of our stack during regression. For $\delta^{18}O$ the agreement is only slightly worse, the regression slope of $\delta^{18}O_{rub}$ against $\delta^{18}O_{sac}$ is 0.96 ($r^2 = 0.96$) or 0.98±0.01 ($r^2 = 0.96$) with uncertainties. Since $\Delta(\delta^{13}C_{rub})$ and $\Delta(\delta^{13}C_{sac})$ are on average recording virtually the same changes it is difficult to image how the species-specific CIE can play a role here. Due to the small amplitudes of the CIE in $\delta^{18}O$ it is yet inconclusive if the CIE plays a role for $\Delta(\delta^{18}O_{rub})$ versus $\Delta(\delta^{18}O_{sac})$.

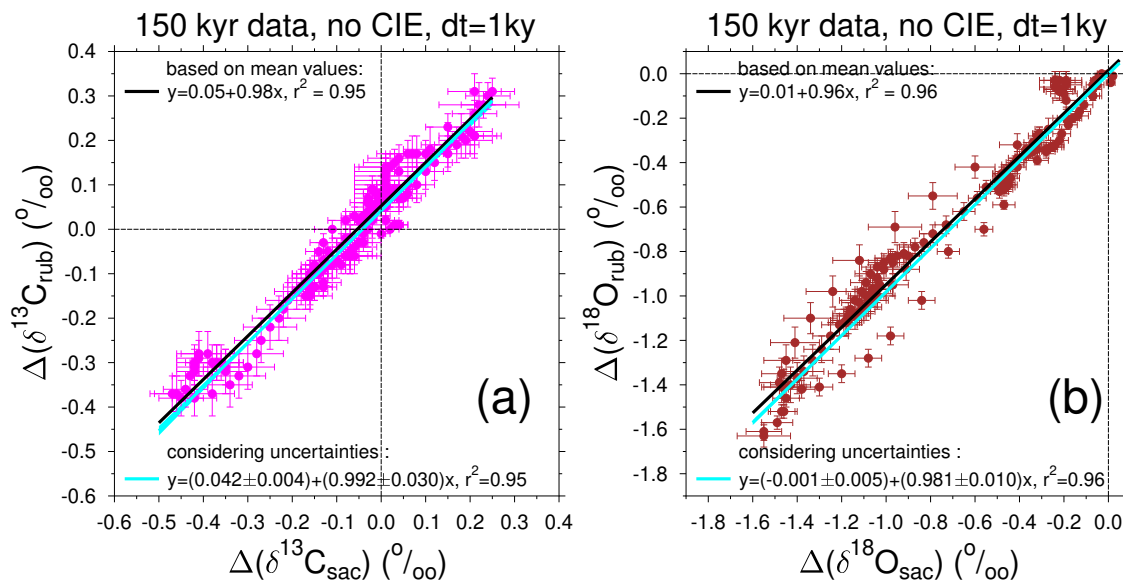**Figure 4.** Scatter plot of our new stacks (a) $\Delta(\delta^{13}C_{rub})$ versus $\Delta(\delta^{13}C_{sac})$ and (b) $\Delta(\delta^{18}O_{rub})$ versus $\Delta(\delta^{18}O_{sac})$. Data stacks without corrections for the CIE are plotted. The time series are restricted to data of last 150 kyr to allow comparison later-on with simulation results which were based on the only 155 kyr long atmospheric $\delta^{13}CO_2$ record. Linear regressions using only the mean values and when using also uncertainties in both x and y are performed.

3 The carbon cycle model BICYCLE-SE

3.1 Brief model description

At the core of BICYCLE — the Box model of the Isotopic Carbon cYCLE — sits a ten boxes large ocean (O) and a terrestrial biosphere consisting of seven boxes (B) together with a one box atmosphere (A), in which the concentration of carbon (as DIC in the ocean, as pCO_2 in the atmosphere, as organic carbon in the biosphere) and both of the isotopes $\delta^{13}C$ and $\Delta^{14}C$ are traced (Köhler et al., 2005). Furthermore, in the ocean alkalinity, PO_4^{3-} as macro-nutrient and O_2 is represented. From the two variables of the marine carbonate system (DIC and alkalinity) all other variables (CO_2, HCO_3^-, CO_3^{2-} and pH) are calculated according to Zeebe and Wolf-Gladrow (2001) with updates of the dissociation constants pK_1 and pK_2 (Mojica Prieto and Millero, 2002). The ten ocean boxes distinguish 100 m deep equatorial (or non-polar) surface waters in Atlantic and Indo-Pacific from 1000 m deep surface ocean boxes in the high latitudes (North Atlantic, Southern Ocean, North Pacific). Here, non-polar boxes range from 40°S to 40°N in the Indo-Pacific and to 50°N in the Atlantic, rather similar to the latitudinal coverage of the sediment cores from which $\Delta(\delta^{13}C_{rub})$ and $\Delta(\delta^{13}C_{sac})$ have been compiled. Deep ocean boxes contain all waters below 1 km in the three basin Atlantic, Southern Ocean, Indo-Pacific. In the equatorial regions the waters between 100
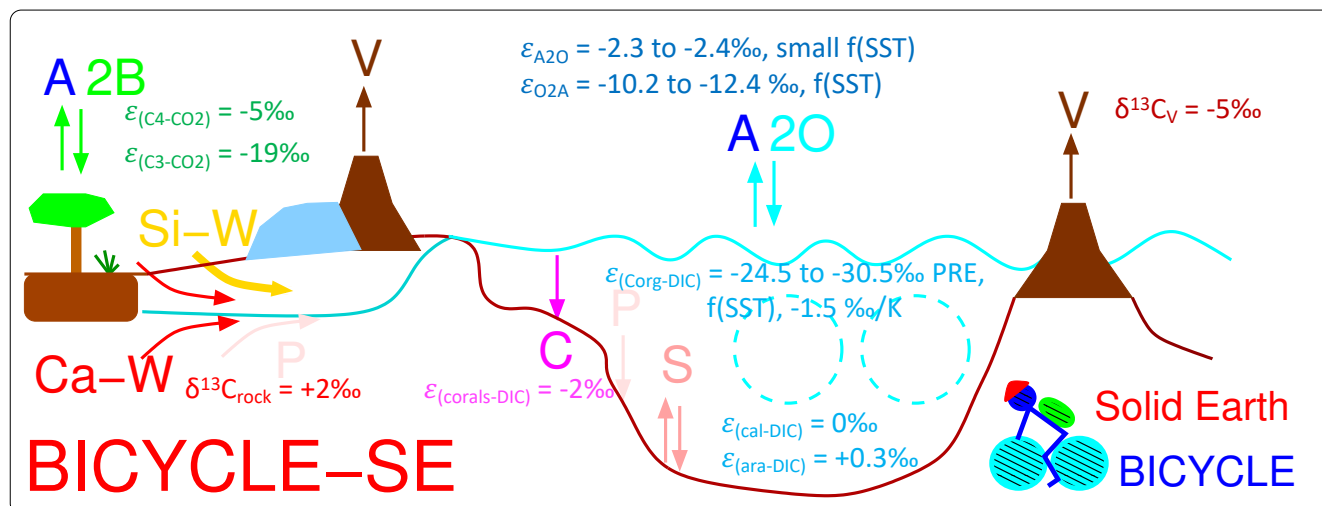
Figure 5. Sketch of the Box model of the isotopic carbon cycle, version solid Earth (BICYCLE-SE), modified from Köhler and Munhoven (2020). V: outgassing of CO_2 from volcanoes on land potentially and temporally overlain by land ice and from hot spot island volcanoes (and mid ocean ridges, not shown) influenced by changing sea level; C: shallow water carbonate deposition due to coral reef growth; Si-W: silicate weathering and Ca-W: carbonate weathering with different sources of C, but both delivering HCO_3^--ions into the ocean; P: PO_4^{3-} riverine input and sedimentary burial; S: $CaCO_3$ sedimentation and dissolution. A2B: atmosphere-biosphere exchange of CO_2; A2O: atmosphere-ocean exchange of CO_2. The cyan-coloured broken circles mimic the two overturning cell in the Atlantic and Indo-Pacific Ocean. The isotopic fractionation ε during exchange processes, or the prescribed $\delta^{13}C$ of external fluxes are given, summarising the parametrisation of the ^{13}C cycle within the model.

and 1000 m water depth are described by intermediate boxes. The terrestrial biosphere (Köhler and Fischer, 2004) distinguishes C_3 and C_4 photosynthesis of grasses and trees, and soil carbon with different turnover times of up to 1000 years.

195   The model extension towards the version BICYCLE-SE used here, that can take care of solid Earth processes, is sketched in Figure 5. The main improvement documented in detail in Köhler and Munhoven (2020) is the implementation of a sediment module, that captures early diagenesis in a 8 cm deep sedimentary mixed layer (M), under which numerous historical layers are implemented. In effect, we now simulate the AOBM subsystem of the global carbon cycle within BICYLE-SE. In each of the three ocean basins (Atlantic; Southern Ocean, Indo-Pacific) the pressure-dependent carbonate system is calculated for

200   every 100 m water depth and depending on the over- or undersaturation of the carbonate-ion concentration $CaCO_3$ is either accumulated or dissolved. Parametrisation and realisation of the sedimentary processes directly follows Munhoven and François (1996) and Munhoven (1997). The carbon isotopes in the sedimentary mixed layer are only followed in aggregated boxes (one for each of the three ocean basin).

    Equipping BICYCLE with a process-based sediment module enables the revised model version BICYCLE-SE to address

205   questions related to changes in solid Earth carbon fluxes in detail and on long-term. Roughly speaking the following processes are considered: 1) CO_2 outgassing from volcanoes on land, hot spot island volcanoes and mid ocean ridge (MOR) hydrothermal

Climate
of the Past
Discussions

activity is realised as partly being dependent on changing sea level. 2) Coral reef growth is a known shallow water carbonate sink, that is to some extent also following sea level rise. 3) Weathering of silicate or carbonate rocks on land, consuming different amounts of atmospheric CO_2, and both leading to bicarbonate fluxes into the ocean. These solid Earth processes are not directly coupled to each other. Their implementation into the model might therefore lead to temporal offsets in various variables, to which the sediment module might react in a carbonate compensation feedback. Further details on the model and the time-dependent forcing are found in Köhler and Munhoven (2020).

3.2 Complete formulation of the ^{13}C cycle in BICYCLE-SE

The following isotopic fractionations are now considered in the BICYCLE-SE model. For this study the whole δ^{13}C cycle has been revised. While isotopic fractionations are given here in the $\varepsilon_{(A-B)}$-notation (in ‰) they are implemented after Zeebe and Wolf-Gladrow (2001) in the model as factors

$$\alpha_{(A-B)} = \frac{\varepsilon_{(A-B)}}{1000} + 1 \tag{1}$$

defined as

$$\alpha_{(A-B)} = \frac{\delta^{13}C_A + 1000}{\delta^{13}C_B + 1000}. \tag{2}$$

There is no convention if the initial or final reservoir is given as A or B here, however here A is always the final and B the initial reservoir of the fractionation process. In some cases a specific process instead of two reservoirs is mentioned in the subscript, e.g. $\varepsilon_{(a2o)}$ and $\varepsilon_{(o2a)}$ for the atmosphere-ocean gas exchange, for which not only the two different reservoirs, but also the direction of the flux plays a role for the size of the isotopic fractionation. In that case the quantified fractionation implies an isotopic depletion connected with the related process for $\varepsilon < 0$‰.

Air-sea gas exchange: Using the measurements from Zhang et al. (1995) we formulate, following in most parts Marchal et al. (1998), for the isotopic fractionation during gas exchange to be consisting of contributions from equilibrium (α^{eq}) and kinetic (α^k) fractionation ($\alpha^{total} = \alpha^{eq} \cdot \alpha^k$). For the atmosphere-to-ocean CO_2 flux a temperature-dependent equilibrium fractionation of $\varepsilon_{a2o}^{eq} = \varepsilon_{(aq-g)}^{eq} = -1.31 + 0.0049 \cdot T_C$ between dissolved (aq) and gaseous (g) CO_2 and a $\varepsilon_{a2o}^k = -1.08$‰ is used. Note, ε_{a2o}^k differs by –0.2‰ from $\varepsilon_{o2a}^k = -0.88$‰ for the ocean-to-atmosphere flux, a necessary correction already given in Zhang et al. (1995), but to our knowledge only rarely applied. For the reverse ocean-to-atmosphere flux we use the equilibrium fractionation $\alpha_{o2a}^{eq} = \alpha_{(aq-DIC)}^{eq} = \sum_i f_i \alpha_{(aq-i)}$ with f_i being the relative shares of CO_2, HCO_3^- and CO_3^{2-} on DIC in the representative ocean box. Furthermore, from the available measurements in Zhang et al. (1995) we derive: $\alpha_{(aq-HCO_3^-)} = \frac{\alpha_{(aq-g)}}{\alpha_{(HCO_3^- - g)}}$, $\alpha_{(aq-CO_3^{2-})} = \frac{\alpha_{(aq-g)}}{\alpha_{(CO_3^{2-} - g)}}$ and $\alpha_{(aq-CO_2)} = 1$ using $\varepsilon_{(CO_3^{2-} - g)} = 7.22 - 0.052 \cdot T_C$ and $\varepsilon_{(HCO_3^- - g)} = 10.78 - 0.114 \cdot T_C$ with T_C being the sea surface temperature in °C.

Marine biology: The pre-industrial marine export production of organic carbon at 100 m water depth is set to 10 PgC/yr (which can increase in glacial periods due to iron fertilisation in the Southern Ocean) with a fixed molar rain ratio of organic C:CaCO$_3$ of 10:1. Existing data on fractionation during marine organic matter production (marine photosynthesis)

are rather weak in determining if and how it depends on CO_2 (Young et al., 2013; Brandenburg et al., 2022; Liu et al., 2022). Furthermore, as discussed in Brandenburg et al. (2022) some species might contain so-called carbon concentrating mechanisms and use not CO_2, but HCO_3^- as source of their carbon, in which case a completely different isotopic fractionation during marine photosynthesis ($\varepsilon_{(C_{org}-DIC)}$) would follow. We base our initial formulation of $\varepsilon_{(C_{org}-DIC)}$ in scenario SEi0 on the data compilation of $\delta^{13}C_{POC}$ in Verwega et al. (2021) who found a dependency on latitude. Using average preindustrial $\delta^{13}C_{DIC}$ of +2.5‰ (Schmittner et al., 2013) as starting values and the $\delta^{13}C_{POC}$ in Verwega et al. (2021) of –22, –24, –28‰ for low, high northern, and high southern latitudes, respectively, and approximating $\varepsilon_{(C_{org}-DIC)} \approx \delta^{13}C_{POC}$ - $\delta^{13}C_{DIC}$, we come up with the following isotopic fractionation $\varepsilon_{(C_{org}-DIC)}$ of $-24.5, -26.5,$ and -30.5‰ accordingly (scenario SEi0). This approximation is motivated by the high uncertainties in $\delta^{13}C_{POC}$ as documented in Verwega et al. (2021).

The breadth in $\delta^{13}C_{POC}$ in the data of Verwega et al. (2021) is huge, ranging from -15 to -35‰. Furthermore, they confirmed the finding of earlier studies (Young et al., 2013; Lorrain et al., 2020) that $\delta^{13}C_{POC}$ becomes much more depleted over time than what is explainable by the ^{13}C Suess effect (Keeling, 1979). In details, between 1960 and 2010 $\delta^{13}C_{POC}$ decreased by about 3 ± 4‰. The Suess Effect shows a decrease in atmospheric $\delta^{13}CO_2$ of about 1.5‰ during that time (Rubino et al., 2013) and it is known that in the ocean the Suess Effect is decreasing with depth (Eide et al., 2017). In the same time, global mean temperature rose by about 0.8 K (Rohde and Hausfather, 2020). This shift in $\delta^{13}C_{POC}$ is probably caused by a shift in the composition of the phytoplankton communities. We therefore use the numbers above as our preindustrial parameter values of $\varepsilon_{(C_{org}-DIC)}$ to which we add a temperature-dependent part of -1.5‰ for any K the sea surface temperature in the relevant surface ocean box disagrees from its preindustrial value (standard scenario SEi). The assumed value fits in the range of recent temperature-dependent $\delta^{13}C_{POC}$ found in Verwega et al. (2021) and has been obtained by tuning to simulate $\delta^{13}CO_2$ at preindustrial times to be similar to its values at LGM, as seen in the ice core data (Figure 3b). This leads to $\varepsilon_{(C_{org}-DIC)}$ at LGM of $-19.3, -20.4, -24.4$‰ for low, high northern, or high southern latitudes, respectively.

Data are also rather uncertain for the isotopic fractionation during the formation of $CaCO_3$. We assume, in agreement with Buitenhuis et al. (2019), that 65% of the $CaCO_3$ exported in the abyss consists of aragonite and 35% of calcite. Calcite is either produced by coccolithophores or planktic foraminifera. Some coccolithophore species suggest an enrichment, others a depletion in $\delta^{13}C$ in their shells with respect to $\delta^{13}C_{DIC}$ in the surrounding water (Ziveri et al., 2003). For planktic foraminifera the CIE is the dominant isotopic fractionation hypothesised to occur during hard shell formation (e.g. Spero et al., 1997, 1999; Russell and Spero, 2000). It is in comparison to $\varepsilon_{(C_{org}-DIC)}$ rather small and species-specific. We therefore choose in the model to set the fractionation during calcite production to be neutral with respect to ^{13}C, thus $\varepsilon_{(cal-DIC)} = 0$‰, but we will consider the CIE in post-processing when comparing simulations with reconstructions. For simplicity and due to missing further evidence for fractionation during aragonite production $\varepsilon_{(ara-DIC)}$ was also kept at 0‰.

The shallow water sink of carbonate in corals is assumed to have a $\delta^{13}C$ that follows after an isotopic fraction of $\varepsilon_{(\text{corals}-\text{DIC})} = -2‰$ from the $\delta^{13}C$ of the DIC in the surface waters. This value is based on a combination of recent data, paleo data from the Great Barrier reef and insights from simulations (Linsley et al., 2019; Felis et al., 2022).

Terrestrial biosphere: On land isotopic fractionation is only assumed to occur during photosynthesis with $\varepsilon_{(\text{C}_3-\text{CO}_2)} =$
275      $-19‰$ and $\varepsilon_{(\text{C}_4-\text{CO}_2)} = -5‰$ for C_3 (all woody plants and some grasses) and C_4 (some other grasses) photosynthesis, respectively (Vogel, 1993; Lloyd and Farquhar, 1994).

External fluxes to the AOBM subsystem: The volcanic CO_2 outgassing flux is assumed to have a fixed $\delta^{13}C$ signature ($\delta^{13}C_V$) of $-5.0‰$, the typical mean value for volcanic outgassing (e.g. Deines, 2002; Roth and Joos, 2012), but note its uncertainty of about $\pm3‰$ around it.

280   From the two weathering fluxes based on either silicate or carbonate rocks, only the latter has a contribution which bring new carbon into the system. Here, 50% of the carbon that as bicarbonate — the weathering product — is entering the ocean with a $\delta^{13}C$ signature ($\delta^{13}C_{\text{rock}}$) of $+2‰$ — identical to the most likely $\delta^{13}C$ values in carbonate rocks build during the Phanerozoic (Bachan et al., 2017). The carbon for the other half of the carbonate weathering flux and for all of the silicate weathering flux is assumed to come from CO_2 in the soil environment. We therefore assume that this CO_2
285   might be dominated by soil respiration fluxes and therefore a $\delta^{13}C$ signature that corresponds to the mean value of the two soil carbon boxes is assumed here.

To balance the inflow of ^{13}C via volcanism and weathering the model has been tuned for long-term stable mean $\delta^{13}C$ values in the AOBM subsystem by the following sink: About 6% of the organic carbon, that is exported from the surface boxes into the abyss is assumed to be lost in the sediment. Note, that this number has been tuned with the previous
290   version of the ^{13}C cycle in operation (Köhler and Munhoven, 2020), but has not been revised thereafter.

In summary, the new parametrisation of the ^{13}C cycle has been implemented as follows: (1) The overall philosophy here is to keep the main carbon cycle untouched, but consider only changes the stable isotope. For this reason, the previously tuned value of organic matter flux into the sediment of about 6% is kept as is, since the strength of this carbon sink also changes the overall C cycle including atmospheric CO_2. (2) Equations for isotopic fractionation during gas exchange are revised from
295   the literature. (3) Fractionation during marine photosynthesis was completely revised and follows in its latitudinal dependency Verwega et al. (2021), is most uncertain and very likely has a temperature-dependency due to species shifts. The size of this temperature-dependency $\varepsilon_{(\text{C}_{\text{org}}-\text{DIC})}$ was tuned to dynamics in atmospheric $\delta^{13}CO_2$ during the last 20 ka. (4) Fractionation during calcite formation is species-specific and roughly neutral. The CIE is therefore only considered in post-processing. (5) All other parameter values, namely fractionation during terrestrial photosynthesis or during coral reef growth, $\delta^{13}C$ of volcanic
300   CO_2 and $\delta^{13}C$ of weathered carbonate rock are also rather uncertainties. However, their chosen parameter values correspond to the means of the reconstructions, and are kept fixed. One might also take alternative approaches by giving more room to uncertainties in other parameter values, or by also reconsidering changes in the main carbon cycle, and not only in the ^{13}C cycle.

Table 1. Overview of simulation scenarios.

Name	Description
SEi	standard run for BICYCLE-SE with updated ^{13}C cycle
SEi0	as SEi, but no temperature-dependent contribution to $\varepsilon_{(C_{org}-DIC)}$
C1	as SEi, but atmospheric $\delta^{13}CO_2$ are prescribed from data (Eggleston et al., 2016a)
C1CO2	as SEi, but atmospheric records ($\delta^{13}CO_2$, CO_2) are prescribed from data (Eggleston et al., 2016a; Köhler et al., 2017a)

3.3 Simulation Setup and Scenarios

305 The BICYCLE-SE model simulates the global carbon cycle as function of changing time-dependent physical boundary conditions (forcing), which are nearly identical to the simulations published in Köhler and Munhoven (2020) and which are also in detail described in that study. Briefly, ocean circulation is prescribed from modern data of the WOCE experiment, while its main temporal changes are restricted to: (a) the Atlantic Meridional Overturning Circulation (AMOC), which is reduced from modern/interglacial 16 Sv to 10 Sv during glacial periods; (b) Southern Ocean (SO) vertical deep mixing is a function of SO

310 sea surface temperature. Ocean and land temperature are prescribed from reconstructions, ocean salinity is varied as function of prescribed sea level. Additionally, aeolian iron input in the SO is assumed to follow dust fluxes measured in Antarctic ice cores, which might change marine biology in the SO from an iron-limited to an iron-unlimited regime, increasing glacial export production of organic matter to the deep ocean. The standard scenario SEi used here is — apart from the revised δ^{13}C cycle — nearly identical to the scenario SE in Köhler and Munhoven (2020). The only difference is that in the application

315 here we revised the applied equatorial SST. It has been based in previous applications on changes in planktic δ^{18}O in only one ODP record. Now we use the SST stack from Barth et al. (2018), which is based on a compilation of SST from 15 non-polar sediment cores. The new equatorial SST forcing is now based on more data, is temporally higher resolved and contains a smaller G/IG amplitude than before. This leads to only minor changes in atmospheric CO_2 of less than 5 ppm, but is important for the ^{13}C cycle, and its temperature-dependencies (isotopic fractionation during atmosphere-ocean gas exchange and during

320 carbon uptake by the marine biology). Simulations are started from interglacial conditions around 210 kyr BP. Scenario SEi0 is only performed to illustrate how the implementation of the temperature-dependency in $\varepsilon_{(C_{org}-DIC)}$ improve the simulated ^{13}C cycle, illustrated by plotting atmospheric $\delta^{13}CO_2$ against data in Figure 6b.

Simulated changes in the atmospheric record are already in scenario SEi not too far away from the reconstructions, especially in CO_2 (Figure 6a). However, to bring the carbon cycle in atmosphere and surface ocean as close as possible to the reconstruc-

325 tions we perform additional simulations in which the atmospheric $\delta^{13}CO_2$ alone (scenario C1) or together with atmospheric CO_2 (scenario C1CO2) is forced by the reconstructions. Here, we use the data splines as plotted in Figure 3a,b (Eggleston et al., 2016a; Köhler et al., 2017a) and ignore the higher resolved data from Taylor Glacier (Menking et al., 2022b), since these more abrupt changes in $\delta^{13}CO_2$ are probably not recorded in our marine sediment records. This implies that internally calculated fluxes are overwritten by changes that are necessary keep the simulated atmospheric carbon variables identical to
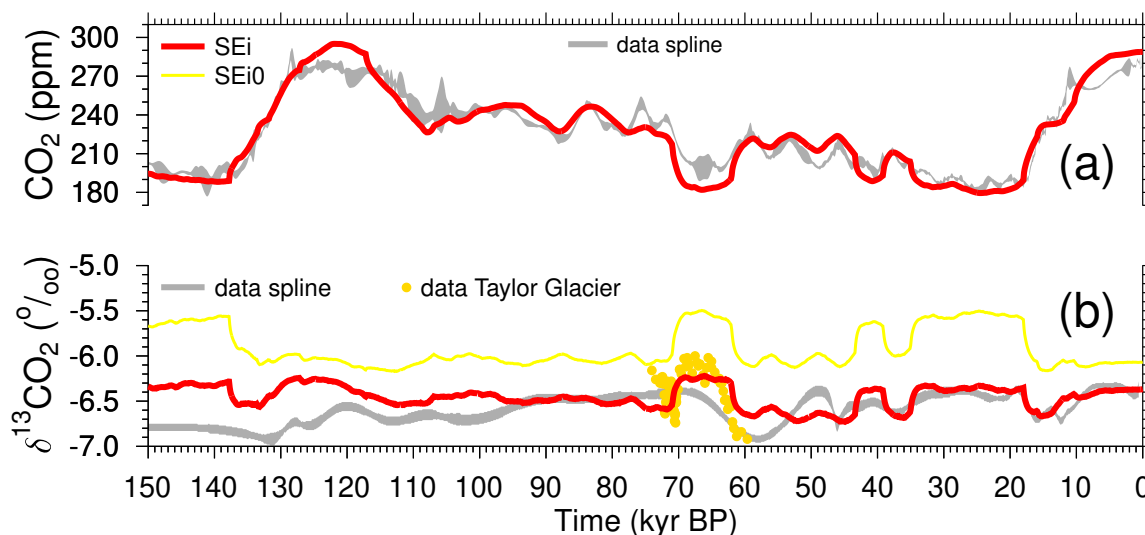
Climate
of the Past
Discussions

Figure 6. Simulation results of atmospheric variables showing reasonable good agreement with (a) CO_2, and necessary improvements in (b) $\delta^{13}CO_2$ during parameter tuning of $\varepsilon_{(C_{org}-DIC)}$. See Table 1 for details of the different scenarios.

330   the reconstructions. This approach is typically applied in CO_2 concentration-driven present day or future ocean carbon cycle simulations (e.g. Hauck et al., 2020). It has already been used in BICYCLE-SE for ^{14}C to obtain radiocarbon in the surface ocean as close to the data as possible during the construction of the most recent marine radiocarbon calibration curve Marine20 (Heaton et al., 2020) and subsequent studies (Köhler et al., 2022). However, since atmospheric CO_2 and $\delta^{13}CO_2$ are normally prognostic variables of the model and their calculated changes should be derived out of the model's differential equations

335   followed by a proper integration scheme, this approach slightly violates the mass conservation. It nevertheless guarantees that simulated surface ocean variables of the carbon cycle are within the model realm as consistent as possible with the atmospheric reconstructions.

4   Results and Discussion

General dynamics of the global carbon cycle in the BICYCLE-SE model have been analysed in detail in Köhler and Munhoven

340   (2020). We here focus on the revised $\delta^{13}C$ cycle, but see how atmospheric CO_2 in scenario SEi meets the ice core data in Figure 6a. Note, that some analysis of $\delta^{13}C$ in the precursor model BICYCLE without solid Earth contributions have been described in Köhler et al. (2010).

4.1   Simulated $\delta^{13}C$ cycle using the BICYCLE-SE model

Atmospheric $\delta^{13}CO_2$ (Eggleston et al., 2016a) is met by the results from scenario SEi only roughly, including some millennial-

345   scale variations around 50–30 kyr BP and the transition from LGM to pre-industrial, shows some deficit the second half of
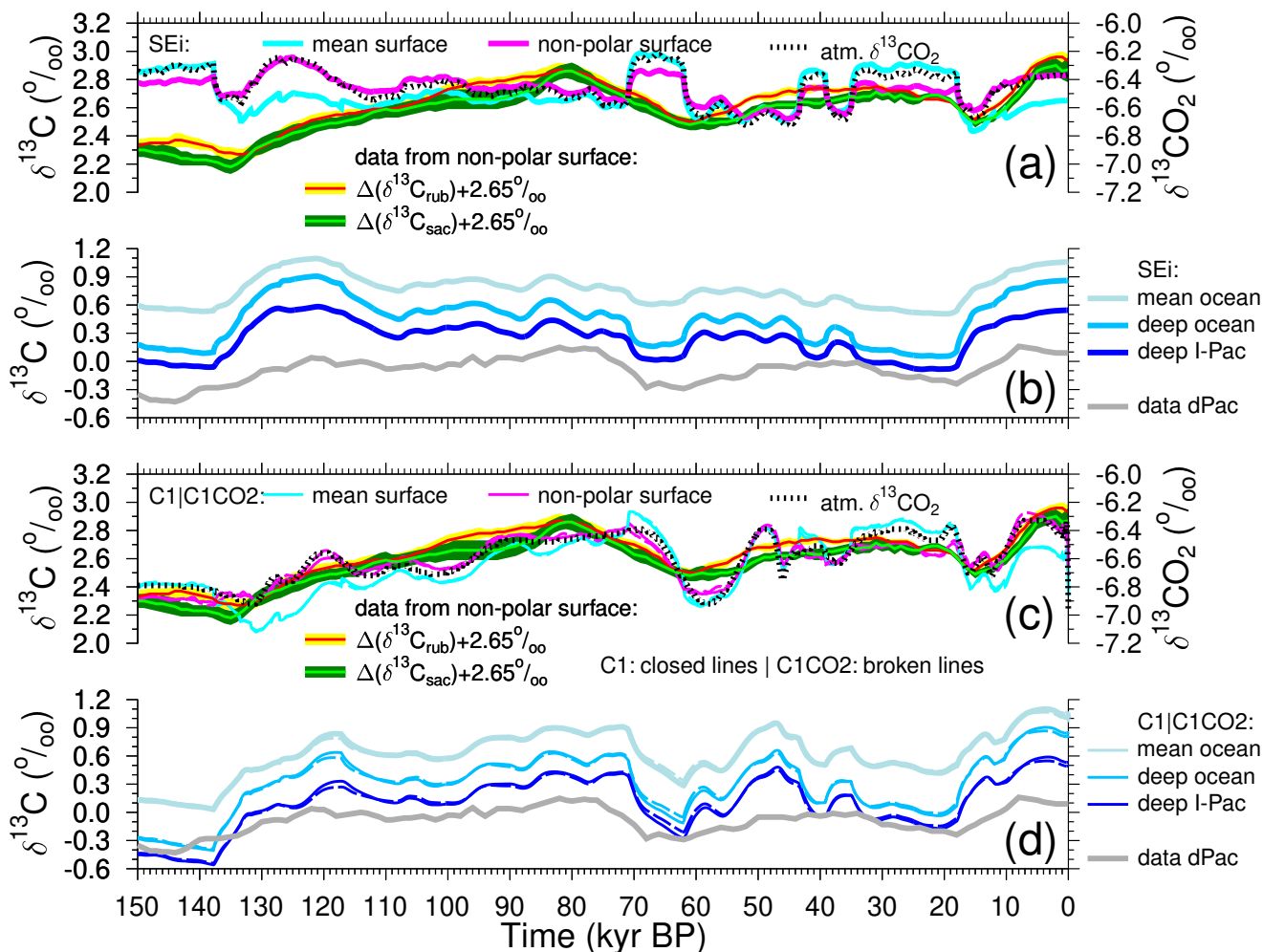
Figure 7. Simulated surface and deeper ocean $\delta^{13}C$ time series from scenario SEi (a, b) and scenarios C1 and C1CO2 (c, d) compared with reconstructions. (a,c) Simulated $\delta^{13}C_{DIC}$ in the global mean surface and in the non-polar surface ocean together with simulated atmospheric $\delta^{13}CO_2$ (right y-axis) are plotted together with our new stacks from the non-polar surface ocean, $\Delta(\delta^{13}C_{rub})$ and $\Delta(\delta^{13}C_{sac})$ shifted by +2.65‰ to meet simulated surface $\delta^{13}C_{DIC}$ at LGM. In (b,d) simulated $\delta^{13}C_{DIC}$ for the deep Indo-Pacific (I-Pac), the mean deep ocean and the mean global ocean are plotted together with $\delta^{13}C$ from benthic foraminifera stacked from six cores in the deep Pacific (dPac) (Lisiecki, 2014). In (c,d) the scenarios C1 (closed lines) and C1CO2 (broken lines) are plotted together. Most of the time the differences between both are so small that lines are indistinguishable.

T1 and in the Holocene (Figure 6b). The PGM-to-LGM trend of 0.45‰ and the minimum around 60 kyr BP are both largely unexplained in this simulation. The attribution of changes in $\delta^{13}CO_2$ to individual processes in the ocean and land carbon cycle has been done before for the precursor model BICYCLE (Köhler et al., 2005, 2010), and is not repeated here, since the misfit to the data indicates some fundamental shortcomings.

Climate
of the Past
Discussions

350   More interesting is how simulated changes in atmospheric $\delta^{13}CO_2$ compares to simulated changes in various marine $\delta^{13}C_{DIC}$ time series (Figure 7). Both global mean surface $\delta^{13}C_{DIC}$ and non-polar surface $\delta^{13}C_{DIC}$ show clear similarities with atmospheric $\delta^{13}CO_2$. Here, non-polar surface values are the mean from the two equatorial ocean boxes, which spatially cover a similar area than the sediment cores used for our new stacks $\Delta(\delta^{13}C_{rub})$ and $\Delta(\delta^{13}C_{sac})$. During glacial times and the onset of deglaciations the dynamics in global mean surface $\delta^{13}C_{DIC}$ are in close agreement with $\delta^{13}CO_2$ in the atmo-
355 sphere, while for the later part of the deglaciations and the interglacials the dynamics in non-polar surface $\delta^{13}C_{DIC}$ fits better to $\delta^{13}CO_2$ in the atmosphere. This difference is probably explained by the dynamics in the polar oceans. During glacial times, the Southern Ocean is highly stratified with little vertical exchange between surface and deep ocean. This stratification breaks down during the terminations and in interglacials allowing faster exchange of tracers between surface and deep ocean leading in the polar oceans to smaller surface-to-deep gradients in $\delta^{13}C_{DIC}$. In other words, the lower deep ocean $\delta^{13}C_{DIC}$ values have
360 a larger impact on polar surface $\delta^{13}C_{DIC}$ during interglacials than during glacials leading to a divergence between $\delta^{13}C_{DIC}$ in the global mean surface and the non-polar surface ocean. The scatter plots between atmospheric $\delta^{13}CO_2$ and either global mean surface or non-polar surface ocean $\delta^{13}C_{DIC}$ show that the latter has the higher correlation (Figure S1, $r^2 = 0.82$ vs. $r^2 = 0.59$, all regression results are complied in Table 2). This implies, that simulations which agree in atmospheric $\delta^{13}CO_2$ with reconstructions (which will be achieved later-on in scenarios C1 and C1CO2) should contain a very likely realisation of
365 $\delta^{13}C_{DIC}$ in the non-polar surface ocean being a perfect target for comparison with our new mono-specific $\delta^{13}C$ stacks. For scenario SEi the misfit in simulated non-polar surface ocean $\delta^{13}C_{DIC}$ and the new $\delta^{13}C$ reconstructions (Figure 7a) is large, but it is yet unclear if this discrepancy can be explained by the CIE or by other processes.

    To understand how representative the reconstructed $\delta^{13}C$ stack from benthic foraminifera in six deep Pacific cores (Lisiecki, 2014) might be we compare it with various different simulated time series: $\delta^{13}C_{DIC}$ in the deep Indo-Pacific, in the mean deep
370 ocean, or in the mean ocean (Figure 7b). Here, deep ocean results from the model refers to ocean boxes that contain waters deeper than 1 km. As expected the deep Indo-Pacific contains the end-member of the $\delta^{13}C$ cycle with the most depleted values. The mean deep ocean $\delta^{13}C_{DIC}$ is offset by 0.2–0.4‰ towards more positive values and shows larger G/IG amplitudes than $\delta^{13}C_{DIC}$ in the deep Indo-Pacific. The mean ocean is again 0.2–0.4‰ more positive in $\delta^{13}C_{DIC}$ than the mean deep ocean with again smaller G/IG amplitudes of 0.53‰ across T1. This number compares $\delta^{13}C_{DIC}$ in the last 6 ka with the mean at the
375 LGM (23–19 ky BP) similarly as in Peterson et al. (2014) who proposed a mean ocean rise in $\delta^{13}C$ by 0.34 ± 0.19‰. However, be aware that in Peterson et al. (2014) the CIE in benthic foraminifera as deduced in Schmittner et al. (2017) is ignored. This suggests that the reconstructions are potentially recording a smaller G/IG change in $\delta^{13}C$ than how $\delta^{13}C_{DIC}$ in the deep ocean might have changed.

    The simulated deep ocean $\delta^{13}C$ is in our simulation results known to be linearly related to simulated atmospheric CO_2 as
380 analysed in Köhler et al. (2010). However, the model misses variations in $\delta^{13}C$ related to periodicities longer than 100-kyr being one main reason for the model/data misfit. This shortcoming is also responsible why when using real world data not deep ocean $\delta^{13}C$, but the $\delta^{13}C$ gradient between the two end members North Atlantic and Pacific needs to taken to match atmospheric CO_2 (Lisiecki, 2010).

Table 2. Linear regression result between various variables. Analysed time series are 150 kyr long with time step between 100 yr and 1 kyr. When needed lower resolved time series are interpolated before analysis. More details are given in the corresponding scatter plots. In column "source" either the simulation scenario or "data" is mentioned with the following data references: 1: this study; 2: Lisiecki and Stern (2016); 3: Lisiecki (2014). Column "Fig." states the label of the figure with the corresponding scatter plot.

Source	x	y	slope	r^2	Fig.
data[1]	$\Delta(\delta^{13}C_{sac})$	$\Delta(\delta^{13}C_{rub})$	0.98	0.95	4a
data[1]	$\Delta(\delta^{13}C_{sac})$	$\Delta(\delta^{13}C_{rub})$	0.99±0.03	0.95	4a
C1CO2	non-polar surface ocean $\delta^{13}C_{DIC}$ + CIE_{sac}	non-polar surface ocean $\delta^{13}C_{DIC}$ + CIE_{rub}	1.26	0.95	S6a
data[1]	$\Delta(\delta^{18}O_{sac})$	$\Delta(\delta^{18}O_{rub})$	0.96	0.96	4b
data[1]	$\Delta(\delta^{18}O_{sac})$	$\Delta(\delta^{18}O_{rub})$	0.98±0.01	0.96	4b
data[2]+C1CO2	mean ocean $\delta^{18}O$ + CIE_{sac}	mean ocean $\delta^{18}O$ + CIE_{rub}	0.97	1.00	S6b
data[1]+SEi	non-polar surface ocean $\delta^{13}C_{DIC}$	$\Delta(\delta^{13}C_{rub})$	-	0.00	S2a
data[1]+SEi	non-polar surface ocean $\delta^{13}C_{DIC}$	$\Delta(\delta^{13}C_{sac})$	-	0.00	S2b
data[1]+C1	non-polar surface ocean $\delta^{13}C_{DIC}$	$\Delta(\delta^{13}C_{rub})$	0.92	0.78	S2c
data[1]+C1	non-polar surface ocean $\delta^{13}C_{DIC}$	$\Delta(\delta^{13}C_{sac})$	0.92	0.78	S2d
data[1]+C1CO2	non-polar surface ocean $\delta^{13}C_{DIC}$	$\Delta(\delta^{13}C_{rub})$	0.92	0.77	S2e
data[1]+C1CO2	non-polar surface ocean $\delta^{13}C_{DIC}$	$\Delta(\delta^{13}C_{sac})$	0.92	0.76	S2f
data[1]+C1CO2	non-polar surface ocean $\delta^{13}C_{DIC}$ + CIE_{rub}	$\Delta(\delta^{13}C_{rub})$	0.45	0.54	S5a
data[1]+C1CO2	non-polar surface ocean $\delta^{13}C_{DIC}$ + CIE_{sac}	$\Delta(\delta^{13}C_{sac})$	0.65	0.67	S5b
data[3]+SEi	deep Indo-Pacific $\delta^{13}C_{DIC}$	deep Pacific $\delta^{13}C_{benthic}$	0.50	0.49	S3a
data[3]+C1	deep Indo-Pacific $\delta^{13}C_{DIC}$	deep Pacific $\delta^{13}C_{benthic}$	0.45	0.78	S3b
data[3]+C1CO2	deep Indo-Pacific $\delta^{13}C_{DIC}$	deep Pacific $\delta^{13}C_{benthic}$	0.47	0.77	S3c
SEi	atm. $\delta^{13}CO_2$	global mean surface ocean $\delta^{13}C_{DIC}$	0.83	0.59	S1a
SEi	atm. $\delta^{13}CO_2$	non-polar surface ocean $\delta^{13}C_{DIC}$	0.66	0.82	S1b
C1	atm. $\delta^{13}CO_2$	global mean surface ocean $\delta^{13}C_{DIC}$	1.11	0.78	S1c
C1	atm. $\delta^{13}CO_2$	non-polar surface ocean $\delta^{13}C_{DIC}$	0.95	0.89	S1d
C1CO2	atm. $\delta^{13}CO_2$	global mean surface ocean $\delta^{13}C_{DIC}$	0.95	0.76	S1e
C1CO2	atm. $\delta^{13}CO_2$	non-polar surface ocean $\delta^{13}C_{DIC}$	0.95	0.88	S1f
C1	atm. CO_2	global mean surface ocean CO_3^{2-}	0.59	0.96	S4a
C1	atm. CO_2	non-polar surface ocean CO_3^{2-}	0.61	0.96	S4b
C1CO2	atm. CO_2	global mean surface ocean CO_3^{2-}	0.63	0.93	S4c
C1CO2	atm. CO_2	non-polar surface ocean CO_3^{2-}	0.65	0.93	S4d

Above we have shown that once changes in the atmospheric $\delta^{13}CO_2$ are met by the simulations the model then also should

385   give a reasonable answer for how $\delta^{13}C_{DIC}$ in the non-polar surface ocean might have looked like. Furthermore, the close agreement of simulated and reconstructed CO_2 suggests that the assumed carbon cycle changes in our approach might be one possible realisation that is not too far away from the truth. However, the misfit between simulation results from scenario SEi and reconstruction in the $\delta^{13}C$ cycle — linear regressions between simulations and reconstructions found no correlation at all (Figure S2a,b) — is not easily fixed. To improve our results we force in the following the model with the atmospheric records

390   (scenario C1: only using $\delta^{13}CO_2$; scenario C1CO2: using both $\delta^{13}CO_2$ and CO_2) to have conditions in the surface ocean as close to reconstructions as possible. Doing so leads to even tighter correlations between simulated atmospheric $\delta^{13}CO_2$ and simulated $\delta^{13}C_{DIC}$ in the surface ocean than what we obtained for scenario SEi, the r^2-correlations between these variables are in scenarios C1 and C1CO2 with prescribed atmospheric $\delta^{13}CO_2$ ≥ 0.76 and ≥ 0.88 for global mean surface $\delta^{13}C_{DIC}$ and non-polar surface $\delta^{13}C_{DIC}$, respectively (Figure S1). Furthermore, in both scenarios the changes in simulated $\delta^{13}C_{DIC}$

395   in the non-polar surface ocean agree remarkably well (r^2 between 0.76 and 0.78, Figure S2c–f) with changes in our new stacks $\Delta(\delta^{13}C_{rub})$ and $\Delta(\delta^{13}C_{sac})$ without consideration of the CIE (Figure 7c), at least on the orbital timescales. Some more abrupt changes contained in the simulations are not recorded in the reconstructions, probably because bioturbation in the surface sediments together with the stacking procedure prevents our marine record from successfully resolving millennial-scale features. Furthermore, deep ocean $\delta^{13}C_{DIC}$ is on orbital time scale now also in better agreement with the data (Figure 7d), —

400   the r^2 of a linear regression between simulated deep Indo-Pacific $\delta^{13}C_{DIC}$ and reconstructed deep Pacific rises from 0.59 for scenario SEi to 0.77 and above for the scenarios forced by atmospheric carbon records (Figure S3), although the rise in mean ocean $\delta^{13}C_{DIC}$ during T1 has now been increased to 0.59‰.

4.2   The importance of the carbonate ion effect for non-polar surface ocean $\delta^{13}C$

Although the initial analysis of our results when forced with atmospheric records already suggests only a minor, if any, role

405   for the CIE in the interpretation of stacked mono-specific $\delta^{13}C$ on orbital timescales, in the following we make a more quantitative assessment. The CIE has not yet been implemented in the ^{13}C cycle of the model, but is only investigated here in post-processing. The carbonate ion concentration of either globally mean surface or non-polar mean surface waters in our simulations are tightly anti-correlated to atmospheric CO_2 ($r^2 \geq 0.93$, Figure S4), which is a consequence of the marine carbonate system (Zeebe and Wolf-Gladrow, 2001). Interestingly, both scenarios C1 and C1CO2 lead to rather similar results

410   here, which suggests that the CO_2 forcing in scenario C1CO2 and its violation of mass conservation, is perturbing the carbon cycle only slightly. To be as close as possible to the reconstructions we nevertheless continue in the following by using results from scenario C1CO2.

Thus, CO_3^{2-} in non-polar surface ocean in the simulation typically falls from maximum glacial values of ~ 320 μmol kg^{-1} to interglacial minimum of ~ 250 μmol kg^{-1} across both Terminations 1 and 2 (Figure 8a). This translates into a potential

415   CIE of about 0.62‰ (Figure 8b) for *G. ruber* when we use the slope of $m = -0.0089$ ‰ per μmol kg^{-1} change in $[CO_3^{2-}]$, and of 0.33‰ for *T. sacculifer* (slope of $m = -0.0047$ ‰ per μmol kg^{-1} change in $[CO_3^{2-}]$ (Spero et al., 1999). The y-axis intercepts of the complete regressions for the CIE is determined in order to have maximum agreement between reconstructions

Climate
of the Past

Discussions

and simulations during the LGM. If we add this CIE to our simulated mean equatorial surface ocean $\delta^{13}C_{DIC}$ (Figure 8c) we
end up with time series, which should compare well with the mono-species stacks of $\Delta(\delta^{13}C_{rub})$ and $\Delta(\delta^{13}C_{sac})$ (Figure 8d).

420 Unfortunately, this is not the case. The r^2 in the linear regressions between CIE-corrected $\delta^{13}C_{DIC}$ in non-polar surface waters
and reconstructions is reduced to 0.55 (*G. ruber*) and 0.67 (*T. sacculifer*), while it had been ≥ 0.76 without CIE correction
(Figures S2,5). Thus, we conclude that both species *G. ruber* and *T. sacculifer* are already good recorders of changes in
$\delta^{13}C_{DIC}$ in non-polar surface ocean waters on orbital timescales, albeit with notable offsets in individual records.

4.3 Carbonate ion effect in $\delta^{18}O$

425 The focus of this study is on stable carbon isotope $\delta^{13}C$. However, during the construction of our mono-specific non-polar
stacks of $\Delta(\delta^{13}C_{rub})$ and $\Delta(\delta^{13}C_{sac})$ the corresponding stacks of $\Delta(\delta^{18}O_{rub})$ and $\Delta(\delta^{18}O_{sac})$ are easily-generated by-
products initially used to cross-check the applied age models. However, these $\delta^{18}O$ data give us the possibility to also have
a closer look on the role of the CIE in the recording of oxygen isotopes in foraminiferal shells. For that effort we need a
background time series of $\delta^{18}O$ which represents the signals when not modified by the CIE. Such a mean $\delta^{18}O$ in the non-
430 polar surface ocean should record the same sea-level related variations than the average global ocean, but might differ in
the recorded temperature effect, if the change in average non-polar sea surface temperature differed from the mean ocean
temperature (MOT) change. Pöppelmeier et al. (2023) showed that the LGM-to-preindustrial times (PRE) change in MOT
derived from the model-based interpretation of noble gas reconstructions in ice cores is 2.1 ± 0.7 K. The reconstructed rise in
MOT is slightly higher when ignoring the effect of past saturation changes on noble gases (Shackleton et al., 2023). The data
435 assimilation effort on LGM temperature changes by Tierney et al. (2020) is broadly in agreement with the MOT change of
Pöppelmeier et al. (2023) and proposes that the tropical (30° S to 30° N) sea surface was around 2.6 K colder at LGM than at
PRE, agreeing within the uncertainties with the MOT change. To a first order we therefore assume that the planktic foraminiera
should record the same temperature effect in $\delta^{18}O$ as contained in the mean ocean. Thus, the global ocean $\delta^{18}O$ calculated
from stacking benthic time series (Lisiecki and Stern, 2016) represents the CIE-free background against which we compare
440 our new $\Delta(\delta^{18}O_{rub})$ and $\Delta(\delta^{18}O_{sac})$ stacks.

From the simulated LGM-to-PRE change in mean non-polar surface ocean CO_3^{2-} of about $-70 \, \mu mol \, kg^{-1}$ (Figure 8e)
and the laboratory-based amplitudes of the CIE (-0.0022 and $-0.0014‰$ change in $\delta^{18}O$ per $\mu mol \, kg^{-1}$ for *G. ruber* and *T.
sacculifer*, respectively (Spero et al., 1999)), we derived that $\Delta(\delta^{18}O_{rub})$ and $\Delta(\delta^{18}O_{sac})$ should record the changes since the
LGM by $+0.15$ and $+0.10 \, ‰$ differently than how $\delta^{18}O$ in the surface waters truly changed (Figure 8f). Compared to the G/IG
445 amplitude in mean ocean $\delta^{18}O$ of $-1.65‰$ (Figure 8g) these potential CIEs represent corrections of -9% and -6%, a difference
by 3% which might be difficult to detect in the paleo records. A linear regression through a scatter plat of $\delta^{18}O + CIE_{rub}$
versus $\delta^{18}O + CIE_{sac}$ has a slope of 0.97 ($r^2 = 1.00$, Figure S6b), which is indistinguishable from the slope obtained from
regression through the data stacks (Figure 4b), while the slope when considering the CIE should move to unity (indicating that
both species were recording the same signal underneath the CIE) if the effect plays an important role during data interpretation.
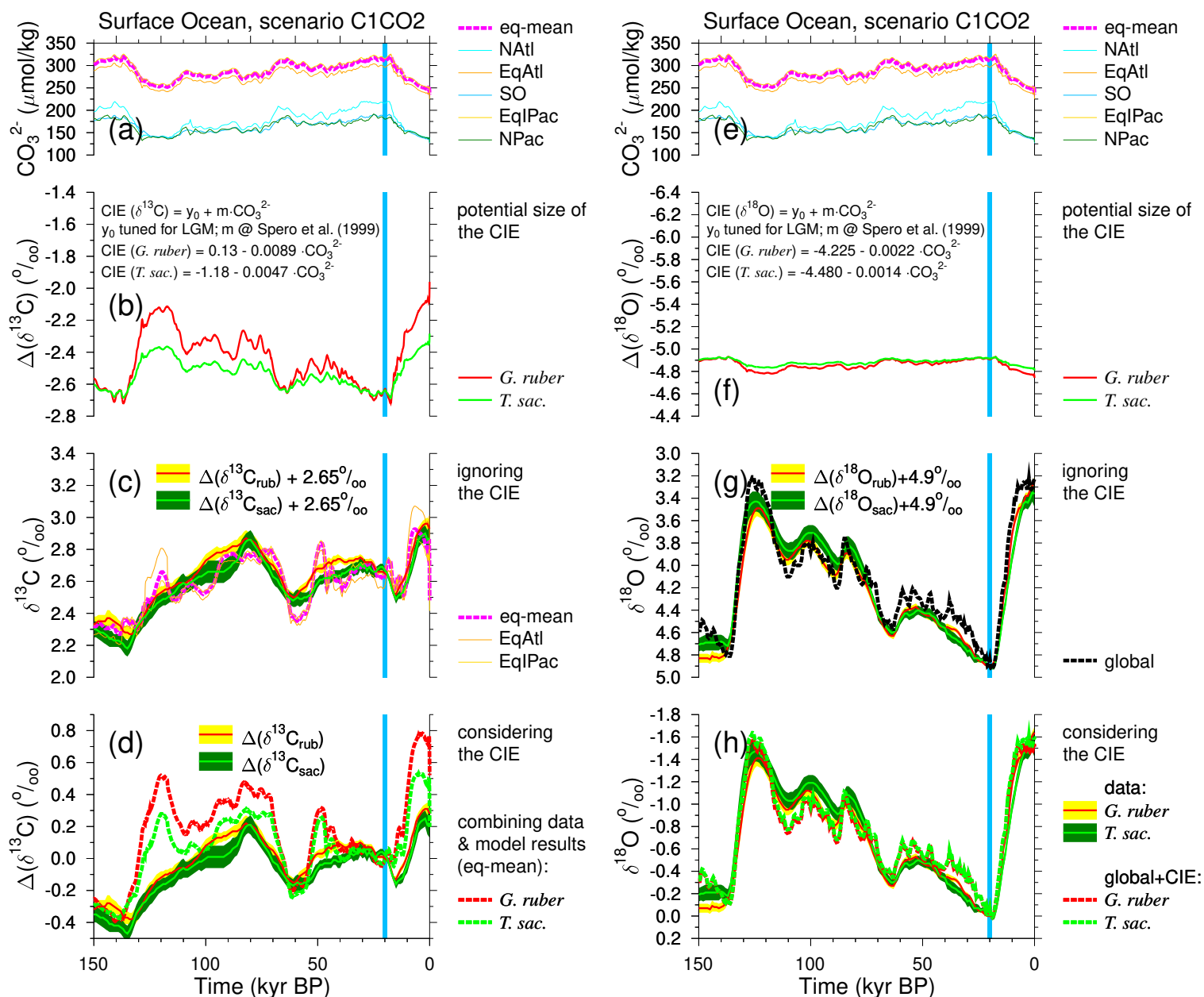450 The evidences for or against the CIE in $\delta^{18}O$ from both data and models are therefore inconclusive.

Figure 8. Calculating the suggested carbonate ion effects (CIE) on *G. ruber* and *T. sacculifer*. Left: effects on δ^{13}C; Right: effects on δ^{18}O. (a,e) surface ocean [CO_3^{2-}]; (b,f) potential CIE using slopes from Spero et al. (1999) (c,g) surface ocean conditions when ignoring the CIE or (d,h) when considering the CIE. Mean anomalies (± 1 SE) of the isotope stacks are calculated with respect to the mean of 21–19 kyr BP (blue vertical band). Simulations use the results from scenario C1CO2. Different surface ocean areas are distinguished: North Atlantic (NAtl, north of 50°N), equatorial Atlantic (EqAtl, 40°S–50°N), Southern Ocean (SO, south of 40°S), equatorial Indo-Pacific (EqIPac, 40°S–40°N), North Pacific (NPac, north of 40°N). The mean non-polar ocean in the model is the mean from the equatorial boxes (eq-mean).

The relative size of the potential CIE on δ^{13}C is much larger. The same $\Delta(CO_3^{2-})$ would lead to 0.62 and 0.33‰ changes in $\delta^{13}C_{rub}$ and $\delta^{13}C_{sac}$, respectively (Figure 8b). When compare to the simulated LGM-to-PRE amplitude of only 0.16‰ in non-polar surface waters (Figure 8g) the CIE-to-G/IG ratios are between a factor of 2 and 4 and CIE signals should clearly stand out in the paleo records.

455 **5 Conclusions**

The CIE for δ^{13}C and δ^{18}O recorded in planktic foraminifera was first identified in laboratory experiments (Spero et al., 1997, 1999), and it was, based on theory, suggested for both isotopes that the underlying processes are directly related to the pH in the surrounding sea water during hard shell formation (Zeebe et al., 1999; Zeebe, 1999). In the here relevant range of pH around 8.0 a linear relation between pH and $[CO_3^{2-}]$ exists (Zeebe and Wolf-Gladrow, 2001). If this theoretical understanding

460 is correct we would expect to see the CIE in neither or both isotopes in the our mono-specific stacks. Thus, although the interpretation of δ^{18}O with respect to the CIE is, due to the signal-to-noise ratio, uncertain we argue, based on the clear evidence of a lack of the CIE in the recording of δ^{13}C in *G. ruber* and *T. sacculifer*, that there is probably also no significant CIE contained in the δ^{18}O time series of both species.

A possible explanation for a lack of a CIE on orbital timescales might be related to homeostasis. In symbiont-bearing planktic

465 foraminifera, such as *G. ruber* and *T. sacculifer*, the pH at the shell surface critically depends on photosynthesis and hence light levels and symbiont density (Jørgensen et al., 1985). In order to facilitate calcification, *G. ruber* and *T. sacculifer* may actively influence the pH at the shell surface by seeking specific (optimum) light levels through vertical migration, thereby keeping the CIE constant over time. Vertical migration to optimise both nutrient uptake and light has been proposed to play an important role in phytoplankton by modelling (Wirtz et al., 2022), an effect which recently has been supported by field data

470 (Zheng et al., 2023). We speculate similar behaviour could occur in the two planktic foraminifera species. It is too early to able able to generalise our finding that on orbital timescales the CIE plays no role for the interpretation of signals in planktic foraminifera in paleo records. For that effort more mono-specific stacks are necessary, preferable from conceptually different foraminifera species without symbionts or spines, as these might potentially show a different behaviour with respect to light (and pH) optimisation. However, our findings might suggest that previous studies on planktic δ^{13}C, which ignored the CIE

475 (e.g. Lynch-Stieglitz et al., 2019; Lund et al., 2019) might not be biased.

Our carbon cycle simulations confirm that atmospheric $\delta^{13}CO_2$ and mean surface ocean $\delta^{13}C_{DIC}$ are tightly related to each other, highlighting the importance of air-sea gas exchange for carbon isotopes. This is not entirely new and has already been discussed before (e.g. Lynch-Stieglitz et al., 2019; Shao et al., 2021; Pinho et al., 2023). However, the ^{13}C cycle is more complex than stated previously (Lynch-Stieglitz et al., 2019; Hu et al., 2020; Pinho et al., 2023) which suggest that one

480 might calculate a mean surface ocean $\delta^{13}C_{DIC}$ as function of atmospheric $\delta^{13}CO_2$ and a temperature-dependent fractionation during gas exchange. We here assumed, based on modern data from Verwega et al. (2021), that species composition and therefore isotopic fractionation during marine photosynthesis might also be temperature-dependent having an important impact

on surface ocean $\delta^{13}C_{DIC}$. Furthermore, our simulation results show that $\delta^{13}C_{DIC}$ in polar and non-polar surface ocean have a different and time-dependent relation to atmospheric $\delta^{13}CO_2$.

485   Finally, since our simulations were forced by atmospheric carbon records we are unable to identify specific processes being responsible for the simulated changes in the ^{13}C cycle. Recent climate simulations (Yun et al., 2023) emphazise the importance of the 405 kyr eccentricity cycle in tropcial hydroclimate. It therefore seems reasonable that the missing long-term variability in $\delta^{13}C$ in our setup might indeed be connected to weathering fluxes as proposed before (e.g. Schneider et al., 2013; Wang et al., 2014), something which needs to be tested in more detail in future carbon cycle simulation studies.

References

Al-Rousan, S., Pätzold, J., Al-Moghrabi, S., and Wefer, G.: Invasion of anthropogenic CO_2 recorded in planktonic foraminifera from the northern Gulf of Aqaba, International Journal of Earth Sciences, 93, 1066–1076, https://doi.org/10.1007/s00531-004-0433-4, 2004.

Bachan, A., Lau, K. V., Saltzman, M. R., Thomas, E., Kump, L. R., and Payne, J. L.: A model for the decrease in amplitude of carbon isotope excursions across the Phanerozoic, American Journal of Science, 317, 641–676, https://doi.org/10.2475/06.2017.01, 2017.

Barth, A. M., Clark, P. U., Bill, N. S., He, F., and Pisias, N. G.: Climate evolution across the Mid-Brunhes Transition, Climate of the Past, 14, 2071–2087, https://doi.org/10.5194/cp-14-2071-2018, 2018.

Bauska, T. K., Baggenstos, D., Brook, E. J., Mix, A. C., Marcott, S. A., Petrenko, V. V., Schaefer, H., Severinghaus, J. P., and Lee, J. E.: Carbon isotopes characterize rapid changes in atmospheric carbon dioxide during the last deglaciation, Proceedings of the National Academy of Sciences, 113, 3465–3470, https://doi.org/10.1073/pnas.1513868113, 2016.

Bereiter, B., Eggleston, S., Schmitt, J., Nehrbass-Ahles, C., Stocker, T. F., Fischer, H., Kipfstuhl, S., and Chappellaz, J.: Revision of the EPICA Dome C CO_2 record from 800 to 600 kyr before present, Geophysical Research Letters, 42, 542–549, https://doi.org/10.1002/2014GL061957, 2015.

Blaauw, M. and Christen, J. A.: Flexible paleoclimate age-depth models using an autoregressive gamma process, Bayesian Analysis, 6, 457 – 474, https://doi.org/10.1214/11-BA618, 2011.

Black, D., Thunell, R., Wejnert, K., and Astor, Y.: Carbon isotope composition of Caribbean Sea surface waters: Response to the uptake of anthropogenic CO2, Geophysical Research Letters, 38, L16 609, https://doi.org/10.1029/2011GL048538, 2011.

Brandenburg, K. M., Rost, B., de Waal, D. B. V., Hoins, M., and Sluijs, A.: Physiological control on carbon fractionation in marine phytoplankton, Biogeosciences, 19, 3305–3315, https://doi.org/10.5194/bg-19-3305-2022, 2022.

Browaeys, J.: Linear fit with both uncertainties in x and in y [code], MATLAB Central File Exchange. https://www.mathworks.com/matlabcentral/fileexchange/45711-linear-fit-with-both-uncertainties-in-x-and-in-y. Last accessed 16th October 2023, 2023.

Buitenhuis, E. T., Le Quéré, C., Bednaršek, N., and Schiebel, R.: Large Contribution of Pteropods to Shallow $CaCO_3$ Export, Global Biogeochemical Cycles, 33, 458–468, https://doi.org/10.1029/2018GB006110, 2019.

Butzin, M., Heaton, T. J., Köhler, P., and Lohmann, G.: A short note on marine reservoir age simulations used in IntCal20, Radiocarbon, 62, 865–871, https://doi.org/10.1017/RDC.2020.9, 2020.

CLIMAP Project Members: CLIMAP 18K Database, IGBP PAGES/World Data Center-A for Paleoclimatology Data Contribution Series 94-001. NOAA/NGDC Paleoclimatology Program, Boulder CO, USA, [data set], https://www.ncei.noaa.gov/pub/data/paleo/paleocean/climap/climap18/, 1994.

Deines, P.: The carbon isotope geochemistry of mantle xenoliths, Earth-Science Reviews, 58, 247 – 278, https://doi.org/10.1016/S0012-8252(02)00064-8, 2002.

Duplessy, J.-C.: (Table 2) Stable carbon and oxygen isotope ratios of Globigerinoides ruber from sediment core MD77-169, PANGAEA, [data set], https://doi.org/10.1594/PANGAEA.726202, 1982.

Eggleston, S., Schmitt, J., Bereiter, B., Schneider, R., and Fischer, H.: Evolution of the stable carbon isotope composition of atmospheric CO_2 over the last glacial cycle, Paleoceanography, 31, 434–452, https://doi.org/10.1002/2015PA002874, 2016a.

Eggleston, S., Schmitt, J., Bereiter, B., Schneider, R., and Fischer, H.: CO_2 concentration and stable isotope ratios of three Antarctic ice cores covering the period from 149.4 - 1.5 kyr before 1950, PANGAEA, [data set], https://doi.org/10.1594/PANGAEA.859181, 2016b.

Eide, M., Olsen, A., Ninnemann, U. S., and Eldevik, T.: A global estimate of the full oceanic ^{13}C Suess effect since the preindustrial, Global Biogeochemical Cycles, 31, 515–534, https://doi.org/10.1002/2016GB005472, 2017.

545 Felis, T., Hinestrosa, G., Köhler, P., and Webster, J. M.: Role of the deglacial buildup of the Great Barrier Reef for the global carbon cycle, Geophysical Research Letters, 49, e2021GL096 495, https://doi.org/10.1029/2021GL096495, 2022.

Fraile, I., Schulz, M., Mulitza, S., and Kucera, M.: Predicting the global distribution of planktonic foraminiera using a dynamic ecosystem model, Biogeosciences, 5, 891–911, 2008.

Ganopolski, A. and Brovkin, V.: Simulation of climate, ice sheets and CO_2 evolution during the last four glacial cycles with an Earth system

550 model of intermediate complexity, Climate of the Past, 13, 1695–1716, https://doi.org/10.5194/cp-13-1695-2017, 2017.

Hauck, J., Zeising, M., Le Quéré, C., Gruber, N., Bakker, D. C. E., Bopp, L., Chau, T. T. T., Gürses, Ö., Ilyina, T., Landschützer, P., Lenton, A., Resplandy, L., Rödenbeck, C., Schwinger, J., and Séférian, R.: Consistency and Challenges in the Ocean Carbon Sink Estimate for the Global Carbon Budget, Frontiers in Marine Science, 7, 852, https://doi.org/10.3389/fmars.2020.571720, 2020.

Heaton, T. J., Köhler, P., Butzin, M., Bard, E., Reimer, R. W., Austin, W. E., Ramsey, C. B., Grootes, P. M., Hughen, K. A., Kromer, B.,

555 Reimer, P. J., Adkins, J. F., Burke, A., Cook, M. S., Olsen, J., and Skinner, L. C.: Marine20 - the marine radiocarbon age calibration curve (0 - 55,000 cal BP), simulated data for IntCal20, PANGAEA, [data set], https://doi.org/10.1594/PANGAEA.914500, 2020.

Heaton, T. J., Köhler, P., Butzin, M., Bard, E., Reimer, R. W., Austin, W. E. N., Ramsey, C. B., Grootes, P. M., Hughen, K. A., Kromer, B., Reimer, P. J., Adkins, J., Burke, A., Cook, M. S., Olsen, J., and Skinner, L. C.: Marine20 — the marine radiocarbon age calibration curve (0–55,000 cal BP), Radiocarbon, 62, 779–820, https://doi.org/10.1017/RDC.2020.68, 2020.

560 Hu, R., Bostock, H. C., Greaves, M., Piotrowski, A. M., and McCave, I. N.: Coupled evolution of stable carbon isotopes between the Southern Ocean and the atmosphere over the last 260 ka, Earth and Planetary Science Letters, 538, 116 215, https://doi.org/10.1016/j.epsl.2020.116215, 2020.

Jørgensen, B. B., Erez, J., Revsbech, P., and Cohen, Y.: Symbiotic photosynthesis in a planktonic foraminiferan, Globigerinoides sacculifer (Brady), studied with microelectrodes1, Limnology and Oceanography, 30, 1253–1267,

565 https://doi.org/https://doi.org/10.4319/lo.1985.30.6.1253, 1985.

Keeling, C. D.: The Suess effect: ^{13}Carbon-^{14}Carbon interrelations, Environment International, 2, 229 – 300, https://doi.org/10.1016/0160-4120(79)90005-9, 1979.

Köhler, P.: Plio-Pleistocene simulations from a global carbon cycle box model, PANGAEA, [data set], https://doi.org/10.1594/PANGAEA.940169, 2022.

570 Köhler, P. and Fischer, H.: Simulating changes in the terrestrial biosphere during the last glacial/interglacial transition, Global and Planetary Change, 43, 33–55, https://doi.org/10.1016/j.gloplacha.2004.02.005, 2004.

Köhler, P. and Mulitza, S.: Mono-specific non-polar stacks of δ^{13}C and δ^{18}O from the planktic foraminifera G. ruber and T. sacculifer and simulation results of the ^{13}C cycle across the last glacial cycle, PANGAEA, registration pending, temporary link to data: https://my.hidrive.com/share/d96gvng3g3, [data set], 2023.

575 Köhler, P. and Munhoven, G.: Late Pleistocene carbon cycle revisited by considering solid Earth processes, Paleoceanography and Paleoclimatology, 35, e2020PA004 020, https://doi.org/10.1029/2020PA004020, 2020.

Köhler, P., Fischer, H., Munhoven, G., and Zeebe, R. E.: Quantitative interpretation of atmospheric carbon records over the last glacial termination, Global Biogeochemical Cycles, 19, GB4020, https://doi.org/10.1029/2004GB002345, 2005.

Köhler, P., Fischer, H., and Schmitt, J.: Atmospheric $\delta^{13}CO_2$ and its relation to pCO_2 and deep ocean δ^{13}C during the late Pleistocene,

580 Paleoceanography, 25, PA1213, https://doi.org/10.1029/2008PA001703, 2010.

Köhler, P., Nehrbass-Ahles, C., Schmitt, J., Stocker, T. F., and Fischer, H.: A 156 kyr smoothed history of the atmospheric greenhouse gases CO_2, CH_4, and N_2O and their radiative forcing, Earth System Science Data, 9, 363–387, https://doi.org/10.5194/essd-9-363-2017, 2017a.

Köhler, P., Nehrbass-Ahles, C., Schmitt, J., Stocker, T. F., and Fischer, H.: Compilations and splined-smoothed calculations of continuous records of the atmospheric greenhouse gases CO_2, CH_4, and N_2O and their radiative forcing since the penultimate glacial maximum,
585   PANGAEA, [data set], https://doi.org/10.1594/PANGAEA.871273, 2017b.

Köhler, P., Adolphi, F., Butzin, M., and Muscheler, R.: Toward reconciling radiocarbon production rates with carbon cycle changes of the last 55,000 years, Paleoceanography and Paleoclimatology, 37, e2021PA004 314, https://doi.org/10.1029/2021PA004314, 2022.

Langner, M. and Mulitza, S.: Technical note: PaleoDataView — a software toolbox for the collection, homogenization and visualization of marine proxy data, Climate of the Past, 15, 2067–2072, https://doi.org/10.5194/cp-15-2067-2019, 2019.

590   Laskar, J., Robutel, P., Joutel, F., Gastineau, M., Correia, A. C. M., and Levrard, B.: A long term numerical solution for the insolation quantities of the Earth, Astronomy and Astrophysics, 428, 261–285, https://doi.org/10.1051/0004-6361:20041335, 2004.

Linsley, B. K., Dunbar, R. B., Dassié, E. P., Tangri, N., Wu, H. C., Brenner, L. D., and Wellington, G. M.: Coral carbon isotope sensitivity to growth rate and water depth with paleo-sea level implications, Nature Communications, 10, 2056, https://doi.org/10.1038/s41467-019-10054-x, 2019.

595   Lisiecki, L. E.: A benthic δ^{13}C-based proxy for atmospheric pCO_2 over the last 1.5 Myr, Geophysical Research Letters, 37, L21 708, https://doi.org/10.1029/2010GL045109, 2010.

Lisiecki, L. E.: Atlantic overturning responses to obliquity and precession over the last 3 Myr, Paleoceanography, 29, 71–86, https://doi.org/10.1002/2013PA002505, 2014.

Lisiecki, L. E. and Raymo, M. E.: A Pliocene-Pleistocene stack of 57 globally distributed benthic δ^{18}O records, Paleoceanography, 20,
600   PA1003, https://doi.org/10.1029/2004PA001071, 2005.

Lisiecki, L. E. and Stern, J. V.: Regional and global benthic δ^{18}O stacks for the last glacial cycle, Paleoceanography, 31, 1368–1394, https://doi.org/10.1002/2016PA003002, 2016.

Liu, Q., Kandasamy, S., Zhai, W., Wang, H., Veeran, Y., Gao, A., and Chen, C.-T. A.: Temperature is a better predictor of stable carbon isotopic compositions in marine particulates than dissolved CO_2 concentration, Communications Earth & Environment, 3, 303,
605   https://doi.org/10.1038/s43247-022-00627-y, 2022.

Lloyd, J. and Farquhar, G. D.: ^{13}C discrimination during CO_2 assimilation by the terrestrial biosphere, Oecologia, 99, 201–215, 1994.

Lorrain, A., Pethybridge, H., Cassar, N., Receveur, A., Allain, V., Bodin, N., Bopp, L., Choy, C. A., Duffy, L., Fry, B., Goñi, N., Graham, B. S., Hobday, A. J., Logan, J. M., Ménard, F., Menkes, C. E., Olson, R. J., Pagendam, D. E., Point, D., Revill, A. T., Somes, C. J., and Young, J. W.: Trends in tuna carbon isotopes suggest global changes in pelagic phytoplankton communities, Global Change Biology, 26,
610   458–470, https://doi.org/10.1111/gcb.14858, 2020.

Lund, D., Hertzberg, J., and Lacerra, M.: Carbon isotope minima in the South Atlantic during the last deglaciation: evaluating the influence of air-sea gas exchange, Environmental Research Letters, 14, 055 004, https://doi.org/10.1088/1748-9326/ab126f, 2019.

Lynch-Stieglitz, J., Valley, S. G., and Schmidt, M. W.: Temperature-dependent ocean-atmosphere equilibration of carbon isotopes in surface and intermediate waters over the deglaciation, Earth and Planetary Science Letters, 506, 466 – 475,
615   https://doi.org/10.1016/j.epsl.2018.11.024, 2019.

Ma, W., Tian, J., Li, Q., and Wang, P.: Simulation of long eccentricity (400-kyr) cycle in ocean carbon reservoir during Miocene Climate Optimum: Weathering and nutrient response to orbital change, Geophysical Research Letters, 38, L10 701, https://doi.org/10.1029/2011GL047680, 2011.

Marchal, O., Stocker, T. F., and Joos, F.: A latitude-depth, circulation-biogeochemical ocean model for paleoclimate studies. Development
620   and sensitivities, Tellus, 50B, 290–316, 1998.

Meinecke, G.: Isotopes (G. sacculifer) of sediment core GeoB1112-4, PANGAEA, [data set], https://doi.org/10.1594/PANGAEA.54765,
        1999.

Menking, J., Shackleton, S., Barker, S., Bauska, T., Brook, E., Buffen, A., Dyonisius, M., Petrenko, V., and Severinghaus, J.: Taylor Glacier
        CO_2 Isotope Data 74-59 kyr, U.S. Antarctic Program (USAP) Data Center, [data set], https://doi.org/10.15784/601600, 2022a.

625   Menking, J. A., Shackleton, S. A., Bauska, T. K., Buffen, A. M., Brook, E. J., Barker, S., Severinghaus, J. P., Dyonisius, M. N., and Petrenko,
        V. V.: Multiple carbon cycle mechanisms associated with the glaciation of Marine Isotope Stage 4, Nature Communications, 13, 5443,
        https://doi.org/10.1038/s41467-022-33166-3, 2022b.

Menviel, L., Joos, F., and Ritz, S.: Simulating atmospheric CO_2, ^{13}C and the marine carbon cycle during the Last Glacial-Interglacial cycle:
        possible role for a deepening of the mean remineralization depth and an increase in the oceanic nutrient inventory, Quaternary Science
630   Reviews, 56, 46 – 68, https://doi.org/10.1016/j.quascirev.2012.09.012, 2012.

Menviel, L., Mouchet, A., Meissner, K. J., Joos, F., and England, M. H.: Impact of oceanic circulation changes on atmospheric $\delta^{13}CO_2$,
        Global Biogeochemical Cycles, 29, 1944–1961, https://doi.org/10.1002/2015GB005207, 2015.

Mojica Prieto, F. J. and Millero, F. J.: The values of $pK_1 + pK_2$ for the dissolution of carbonic acid in seawater, Geochimica et Cosmochimica
        Acta, 66, 2529–2540, https://doi.org/10.1016/S0016-7037(02)00855-4, 2002.

635   Mulitza, S., Bickert, T., Bostock, H. C., Chiessi, C. M., Donner, B., Govin, A., Harada, N., Huang, E., Johnstone, H. J. H., Kuhnert,
        H., Langner, M., Lamy, F., Lembke-Jene, L., Lisiecki, L. E., Lynch-Stieglitz, J., Max, L., Mohtadi, M., Mollenhauer, G., Muglia, J.,
        Nürnberg, D., Paul, A., Rühlemann, C., Repschläger, J., Saraswat, R., Schmittner, A., Sikes, E. L., Spielhagen, R. F., and Tiedemann, R.:
        World Atlas of late Quaternary Foraminiferal Oxygen and Carbon Isotope Ratios (WA_Foraminiferal_Isotopes_2022), PANGAEA, [data
        set], https://doi.org/10.1594/PANGAEA.936747, 2021.

640   Mulitza, S., Bickert, T., Bostock, H. C., Chiessi, C. M., Donner, B., Govin, A., Harada, N., Huang, E., Johnstone, H., Kuhnert, H., Langner,
        M., Lamy, F., Lembke-Jene, L., Lisiecki, L., Lynch-Stieglitz, J., Max, L., Mohtadi, M., Mollenhauer, G., Muglia, J., Nürnberg, D., Paul,
        A., Rühlemann, C., Repschläger, J., Saraswat, R., Schmittner, A., Sikes, E. L., Spielhagen, R. F., and Tiedemann, R.: World Atlas of late
        Quaternary Foraminiferal Oxygen and Carbon Isotope Ratios, Earth System Science Data, 14, 2553–2611, https://doi.org/10.5194/essd-
        14-2553-2022, 2022.

645   Munhoven, G.: Modelling glacial-interglacial atmospheric CO_2 variations: the role of continental weathering, Ph.D. thesis, Université de
        Liège, Liège, Belgium, http://hdl.handle.net/2268/161314, 1997.

Munhoven, G. and François, L. M.: Glacial-interglacial variability of atmospheric CO_2 due to changing continental silicate rock weathering:
        a model study, Journal of Geophysical Research, 101(D16), 21 423–21 437, https://doi.org/10.1029/96JD01842, 1996.

Nederbragt, A. J.: The Effect of Seawater Carbonate Chemistry on the Stable Isotope Composition of Cibicidoides wuellerstorfi and Other
650   Cibicidoides Species, Paleoceanography and Paleoclimatology, 38, e2023PA004 667, https://doi.org/10.1029/2023PA004667, 2023.

Oliver, K. I. C., Hoogakker, B. A. A., Crowhurst, S., Henderson, G. M., Rickaby, R. E. M., Edwards, N. R., and Elderfield, H.: A synthesis
        of marine sediment core δ^{13}C data over the last 150 000 years, Climate of the Past, 6, 645–673, https://doi.org/10.5194/cp-6-645-2010,
        2010.

Oppo, D. W. and Fairbanks, R. G.: Carbon isotope composition of tropcial surface water during the past 22,000 years, Paleoceanography, 4,
655   333–351, https://doi.org/10.1029/PA004i004p00333, 1989.

Paillard, D.: The Plio-Pleistocene climatic evolution as a consequence of orbital forcing on the carbon cycle, Climate of the Past, 13, 1259–1267, https://doi.org/10.5194/cp-13-1259-2017, 2017.

Pälike, H., Norris, R. D., Herrle, J. O., Wilson, P. A., Coxall, H. K., Lear, C. H., Shackleton, N. J., k. Tripati, A., and Wade, B. S.: The heartbeat of the Oligocene climate system, Science, 314, 1894–1898, doi: 10.1126/science.1133 822, 2006.

660   Peterson, C. D. and Lisiecki, L. E.: Deglacial carbon cycle changes observed in a compilation of 127 benthic δ^{13}C time series (20–6 ka), Climate of the Past, 14, 1229–1252, https://doi.org/10.5194/cp-14-1229-2018, 2018.

Peterson, C. D., Lisiecki, L. E., and Stern, J. V.: Deglacial whole-ocean δ^{13}C change estimated from 480 benthic foraminiferal records, Paleoceanography, 29, 549–563, https://doi.org/10.1002/2013PA002552, 2014.

Pinho, T., Chiessi, C. M., Campos, M. C., Portilho-Ramos, R. C., Martínez-Méndez, G., Venancio, I. M., Nascimento, R. A., Crivel-
665   lari, S., Albuquerque, A. L., Arz, H. W., Tiedemann, R., Bahr, A., and Mulitza, S.: Thermodynamic air-sea equilibration controls carbon isotopic composition of the South Atlantic thermocline during the last glacial period, Global and Planetary Change, 229, 104 223, https://doi.org/10.1016/j.gloplacha.2023.104223, 2023.

Pöppelmeier, F., Baggenstos, D., Grimmer, M., Liu, Z., Schmitt, J., Fischer, H., and Stocker, T. F.: The Effect of Past Saturation Changes on Noble Gas Reconstructions of Mean Ocean Temperature, Geophysical Research Letters, 50, e2022GL102 055,
670   https://doi.org/https://doi.org/10.1029/2022GL102055, 2023.

Reimer, P. J., Austin, W. E. N., Bard, E., Bayliss, A., Blackwell, P. G., Bronk Ramsey, C., Butzin, M., Cheng, H., Edwards, R. L., Friedrich, M., Grootes, P. M., Guilderson, T. P., Hajdas, I., Heaton, T. J., Hogg, A. G., Hughen, K. A., Kromer, B., Manning, S. W., Muscheler, R., Palmer, J. G., Pearson, C., van der Plicht, H., Reimer, R. W., Richards, D. A., Scott, E. M., Southon, J. R., Turney, C. S. M., Wacker, L., Adophi, F., Büntgen, U., Capano, M., Fahrni, S., Fogtmann-Schulz, A., Friedrich, R., Köhler, P., Kudsk, S., Miyake, F., Olsen, J., Reinig,
675   F., Sakamoto, M., Sookdeo, A., and Talamo, S.: The IntCal20 Northern Hemisphere radiocarbon age calibration curve (0–55 cal kBP), Radiocarbon, 62, 725–757, https://doi.org/10.1017/RDC.2020.41, 2020.

Rohde, R. A. and Hausfather, Z.: The Berkeley Earth Land/Ocean Temperature Record, Earth System Science Data, 12, 3469—3479, 2020.

Romahn, S.: Western Indian Ocean circulation and climate variability on different time scales: a study based on stable oxygen and carbon isotopes, benthic foraminiferal assemblages and Mg/Ca paleothermometry, PhD thesis, Fachbereich Geowissenschaften, Universität
680   Bremen, 95 pp., 2014.

Roth, R. and Joos, F.: Model limits on the role of volcanic carbon emissions in regulating glacial-interglacial CO_2 variations, Earth and Planetary Science Letters, 329 - 330, 141 – 149, https://doi.org/10.1016/j.epsl.2012.02.019, 2012.

Rubino, M., Etheridge, D. M., Trudinger, C. M., Allison, C. E., Battle, M. O., Langenfelds, R. L., Steele, L. P., Curran, M., Bender, M., White, J. W. C., Jenk, T. M., Blunier, T., and Francey, R. J.: A revised 1000-year atmospheric δ^{13}C-CO_2 record from Law Dome and
685   South Pole, Antarctica, Journal of Geophysical Research: Atmospheres, 118, 8482–8499, https://doi.org/10.1002/jgrd.50668, 2013.

Russell, A. D. and Spero, H. J.: Field examination of the oceanic carbonate ion effect on stable isotopes in planktonic foraminifera, Paleoceanography, 15, 43–52, https://doi.org/https://doi.org/10.1029/1998PA000312, 2000.

Russon, T., Paillard, D., and Elliot, M.: Potential origins of 400-500 kyr periodicities in the ocean carbon cycle: A box model approach, Global Biogeochemical Cycles, 24, GB2013, https://doi.org/doi: 10.1029/2009GB003586, 2010.

690   Schmitt, J., Schneider, R., Elsig, J., Leuenberger, D., Lourantou, A., Chappellaz, J., Köhler, P., Joos, F., Stocker, T. F., Leuen-berger, M., and Fischer, H.: Carbon isotope constraints on the deglacial CO_2 rise from ice cores, Science, 336, 711–714, https://doi.org/10.1126/science.1217161, 2012.

Schmittner, A., Gruber, N., Mix, A. C., Key, R. M., Tagliabue, A., and Westberry, T. K.: Biology and air-sea gas exchange controls on the distribution of carbon isotope ratios (δ^{13}C) in the ocean, Biogeosciences, 10, 5793–5816, https://doi.org/10.5194/bg-10-5793-2013, 2013.

695 Schmittner, A., Bostock, H. C., Cartapanis, O., Curry, W. B., Filipsson, H. L., Galbraith, E. D., Gottschalk, J., Herguera, J. C., Hoogakker, B., Jaccard, S. L., Lisiecki, L. E., Lund, D. C., Martínez-Méndez, G., Lynch-Stieglitz, J., Mackensen, A., Michel, E., Mix, A. C., Oppo, D. W., Peterson, C. D., Repschläger, J., Sikes, E. L., Spero, H. J., and Waelbroeck, C.: Calibration of the carbon isotope composition (δ^{13}C) of benthic foraminifera, Paleoceanography, 32, 512–530, https://doi.org/10.1002/2016PA003072, 2017.

Schneider, R., Schmitt, J., Köhler, P., Joos, F., and Fischer, H.: A reconstruction of atmospheric carbon dioxide and its stable car-
700 bon isotopic composition from the penultimate glacial maximum to the last glacial inception, Climate of the Past, 9, 2507–2523, https://doi.org/10.5194/cp-9-2507-2013, 2013.

Shackleton, S., Seltzer, A., Baggenstos, D., and Lisiecki, L. E.: Benthic δ^{18}O records Earth's energy imbalance, Nature Geoscience, 16, 797–802, https://doi.org/10.1038/s41561-023-01250-y, 2023.

Shao, J., Stott, L. D., Menviel, L., Ridgwell, A., Ödalen, M., and Mohtadi, M.: The atmospheric bridge communicated the δ^{13}C decline
705 during the last deglaciation to the global upper ocean, Climate of the Past, 17, 1507–1521, https://doi.org/10.5194/cp-17-1507-2021, 2021.

Slowey, N. C.: The modern and glacial thermoclines along the Bahama Banks, PhD thesis, Massachusetts Institute of Technology and Woods Hole Oceanographic Institution, 1990.

Smith, H. J., Fischer, H., Wahlen, M., Mastroianni, D., and Deck, B.: Dual modes of the carbon cycle since the Last Glacial Maximum,
710 Nature, 400, 248–250, 1999.

Spero, H. J.: Do planktic foraminifera accurately record shifts in the carbon isotopic composition of seawater ΣCO2?, Marine Micropaleon-tology, 19, 275–285, https://doi.org/https://doi.org/10.1016/0377-8398(92)90033-G, 1992.

Spero, H. J. and Lea, D. W.: Intraspecific stable isotope variability in the planktic foraminiferaGlobigerinoides sacculifer: Results from laboratory experiments, Marine Micropaleontology, 22, 221–234, https://doi.org/https://doi.org/10.1016/0377-8398(93)90045-Y, 1993.

715 Spero, H. J. and Williams, D. F.: Extracting environmental information from planktonic foraminiferal δ13C data, Nature, 335, 717–719, https://doi.org/10.1038/335717a0, 1988.

Spero, H. J. and Williams, D. F.: Opening the carbon isotope "vital effect" black box 1. Seasonal temperatures in the euphotic zone, Paleo-ceanography, 4, 593–601, https://doi.org/https://doi.org/10.1029/PA004i006p00593, 1989.

Spero, H. J., Lerche, I., and Williams, D. F.: Opening the carbon isotope 'vital effect' black box, 2, Quantitative model for interpreting
720 foraminiferal carbon isotope data, Paleoceanography, 6, 639–655, https://doi.org/10.1029/91PA02022, 1991.

Spero, H. J., Bijma, J., Lea, D. W., and Bemis, B. E.: Effect of seawater carbonate concentration on foraminiferal carbon and oxygen isotopes, Nature, 390, 497–500, https://doi.org/10.1038/37333, 1997.

Spero, H. J., Bijma, J., Lea, D. W., and Russell, A. D.: Deconvolving Glacial Ocean Carbonate Chemistry from the Planktonic Foraminifera Carbon Isotope Record, in: Reconstructing Ocean History: A Window into the Future, edited by Abrantes, F. and Mix, A. C., pp. 329–342,
725 Springer US, Boston, MA, https://doi.org/10.1007/978-1-4615-4197-4_19, 1999.

Tierney, J. E., Zhu, J., King, J., Malevich, S. B., Hakim, G. J., and Poulsen, C. J.: Glacial cooling and climate sensitivity revisited, Nature, 584, 569–573, https://doi.org/10.1038/s41586-020-2617-x, 2020.

Verwega, M.-T., Somes, C. J., Schartau, M., Tuerena, R. E., Lorrain, A., Oschlies, A., and Slawig, T.: Description of a global marine particulate organic carbon-13 isotope data set, Earth System Science Data, 13, 4861–4880, https://doi.org/10.5194/essd-13-4861-2021,
730 2021.

Vogel, J. C.: Variability of carbon isotope fractionation during photosynthesis, in: Stable isotopes and plant carbon–water relations, edited by Ehleringer, J. R., Hall, A. E., and Farquhar, G. D., pp. 29–46, Academic Press, San Diego, USA, 1993.

Wang, P., Li, Q., Tian, J., Jian, Z., Liu, C., Li, L., and Ma, W.: Long-term cycles in the carbon reservoir of the Quaternary ocean: a perspective from the South China Sea, National Science Review, 1, 119–143, https://doi.org/10.1093/nsr/nwt028, 2014.

735   Wirtz, K., Smith, S. L., Mathis, M., and Taucher, J.: Vertically migrating phytoplankton fuel high oceanic primary production, Nature Climate Change, 12, 750–756, https://doi.org/10.1038/s41558-022-01430-5, 2022.

Wolf-Gladrow, D. A., Bijma, J., and Zeebe, R. E.: Model simulation of the carbonate chemistry in the microenvironment of symbiont bearing foraminifera, Marine Chemistry, 64, 181–198, https://doi.org/10.1016/S0304-4203(98)00074-7, 1999.

Young, J. N., Bruggeman, J., Rickaby, R. E. M., Erez, J., and Conte, M.: Evidence for changes in carbon isotopic fractionation by phyto-
740   plankton between 1960 and 2010, Global Biogeochemical Cycles, 27, 505–515, https://doi.org/https://doi.org/10.1002/gbc.20045, 2013.

Yun, K.-S., Timmermann, A., Lee, S.-S., Willeit, M., Ganopolski, A., and Jadhav, J.: A transient coupled general circulation model (CGCM) simulation of the past 3 million years, Climate of the Past, 19, 1–36, https://doi.org/10.5194/cp-19-1951-2023, 2023.

Zahn-Knoll, R.: Spätquatäre Entwicklung von Küstenauftrieb und Tiefenwasserzirkulation im Nordost-Atlantik. Rekonstruktion anhand stabiler Isotope kalkschaliger Foraminiferen, PhD thesis, Christian-Albrechts-Universität zu Kiel, 111 pp., 1986.

745   Zeebe, R. E.: An explanation of the effect of seawater carbonate concentration on foraminiferal oxygen isotopes, Geochimica et Cosmochimica Acta, 63, 2001–2007, https://doi.org/10.1016/S0016-7037(99)00091-5, 1999.

Zeebe, R. E. and Wolf-Gladrow, D. A.: CO_2 in Seawater: Equilibrium, Kinetics, Isotopes, vol. 65 of *Elsevier Oceanography Book Series*, Elsevier Science Publishing, Amsterdam, The Netherlands, 2001.

Zeebe, R. E., Bijma, J., and Wolf-Gladrow, D. A.: A diffusion-reaction model of carbon isotope fractionation in foraminifera, Marine
750   Chemistry, 64, 199–227, https://doi.org/10.1016/S0304-4203(98)00075-9, 1999.

Zhang, J., Quay, P. D., and Wilbur, D. O.: Carbon isotope fractionation during gas-water exchange and dissolution of CO_2, Geochimica et Cosmochimica Acta, 59, 107–114, 1995.

Zheng, B., Lucas, A. J., Franks, P. J. S., Schlosser, T. L., Anderson, C. R., Send, U., Davis, K., Barton, A. D., and Sosik, H. M.: Dinoflagellate vertical migration fuels an intense red tide, Proceedings of the National Academy of Sciences, 120, e2304590120,
755   https://doi.org/10.1073/pnas.2304590120, 2023.

Ziveri, P., Stoll, H., Probert, I., Klaas, C., Geisen, M., Ganssen, G., and Young, J.: Stable isotope 'vital effects' in coccolith calcite, Earth and Planetary Science Letters, 210, 137–149, https://doi.org/https://doi.org/10.1016/S0012-821X(03)00101-8, 2003.

Original references of the data contributing to our stacks (cited in Table S1 of the Supplement)

Adegbie, A., Schneider, R., Röhl, U., and Wefer, G.: Glacial millennial-scale fluctuations in central African precipitation recorded in ter-

760   rigenous sediment supply and freshwater signals offshore Cameroon, Palaeogeography, Palaeoclimatology, Palaeoecology, 197, 323–333,
https://doi.org/10.1016/S0031-0182(03)00474-7, 2003.

Adegbie, A. T.: Reconstruction of paleoenvironmental conditions in Equatorial Atlantic and the Gulf of Guinea Basins for the last 245.000
years., PhD thesis, Berichte aus dem Fachbereich Geowissenschaften der Universität Bremen, 178, 113 pp., 2001.

Andres, M. S.: Late quaternary paleoceanography of the Great Australian Bight: A geochemical and sedimentological study of cool-water

765   carbonates, ODP Leg 182, Site 1127, PhD thesis, Swiss Federal Institute of Technology Zurich, Switzerland, 2002.

Arz, H. W., Pätzold, J., and Wefer, G.: Correlated Millennial-Scale Changes in Surface Hydrography and Terrigenous Sediment Yield Inferred
from Last-Glacial Marine Deposits off Northeastern Brazil, Quaternary Research, 50, 157–166, https://doi.org/10.1006/qres.1998.1992,
1998.

Arz, H. W., Pätzold, J., and Wefer, G.: The deglacial history of the western tropical Atlantic as inferred from high resolution stable isotope

770   records off northeastern Brazil, Earth and Planetary Science Letters, 167, 105–117, https://doi.org/10.1016/S0012-821X(99)00025-4,
1999a.

Arz, H. W., Pätzold, J., and Wefer, G.: Climatic changes during the last deglaciation recorded in sediment cores from the northeastern
Brazilian Continental Margin, Geo-Marine Letters, 19, 209–218, https://doi.org/10.1007/s003670050111, 1999b.

Ausin, B., Haghipour, N., Wacker, L., Voelker, A. H. L., Hodell, D., Magill, C., Looser, N., Bernasconi, S. M., and Eglinton, T. I.: Radiocarbon

775   Age Offsets Between Two Surface Dwelling Planktonic Foraminifera Species During Abrupt Climate Events in the SW Iberian Margin,
Paleoceanography and Paleoclimatology, 34, 63–78, https://doi.org/10.1029/2018PA003490, 2019.

Bostock, H. C., Opdyke, B. N., Gagan, M. K., and Fifield, L. K.: Carbon isotope evidence for changes in Antarctic Intermediate Water circula-
tion and ocean ventilation in the southwest Pacific during the last glaciation, Paleoceanography, 19, PA4013, doi: 10.1029/2004PA001 047,
2004.

780 Chen, M.-T., Shiau, L.-J., Yu, P.-S., Chiu, T.-C., Chen, Y.-G., and Wei, K.-Y.: 500 000-Year records of carbonate, organic carbon, and
foraminiferal sea-surface temperature from the southeastern South China Sea (near Palawan Island), Palaeogeography, Palaeoclimatology,
Palaeoecology, 197, 113–131, https://doi.org/10.1016/S0031-0182(03)00389-4, 2003.

CLIMAP Project Members: Seasonal reconstructions of the earth's surface at the last glacial maximum, Map and chart series (Geological
Society of America), Geological Society of America, Boulder, Colo., 1981.

785 Curry, W. B. and Crowley, T. J.: The δ^{13}C of equatorial Atlantic surface waters: implications for ice age pCO$_2$ levels, Paleoceanography, 2,
489–517, https://doi.org/10.1029/PA002i005p00489, 1987.

Curry, W. B., Marchitto, T. M., Mcmanus, J. F., Oppo, D. W., and Laarkamp, K. L.: Millennial-scale Changes in Ventilation of the Ther-
mocline, Intermediate, and Deep Waters of the Glacial North Atlantic, vol. 112 of *Geophysical Monograph Series*, pp. 59–76, American
Geophysical Union (AGU), https://doi.org/10.1029/GM112p0059, 1999.

790 De Deckker, P., Moros, M., Perner, K., and Jansen, E.: Influence of the tropics and southern westerlies on glacial interhemispheric asymmetry,
Nature Geoscience, 5, 266–269, https://doi.org/10.1038/ngeo1431, 2012.

Duplessy, J.: North Atlantic deep water circulation during the last climate cycle, Bulletin de l'Institut de Geologie du Bassin d'Aquitaine, 31,
371–391, 1982.

Climate
of the Past
Discussions

Duplessy, J., Bard, E., Arnold, M., Shackleton, N., Duprat, J., and Labeyrie, L.: How fast did the ocean—atmosphere system run during the
795   last deglaciation?, Earth and Planetary Science Letters, 103, 27–40, https://doi.org/10.1016/0012-821X(91)90147-A, 1991.

Dupont, L. and Kuhlmann, H.: Glacial-interglacial vegetation change in the Zambezi catchment, Quaternary Science Reviews, 155, 127–135,
       https://doi.org/10.1016/j.quascirev.2016.11.019, 2017.

Dürkoop, A.: Der Brasil-Strom im Spatquartär: Rekonstruktion der oberflächennahen Hydrographie während der letzten 400 000 Jahre, PhD
       thesis, Berichte aus dem Fachbereich Geowissenschaften der Universität Bremen, 119, 121 pp., 1998.

800   Dürkoop, A., Hale, W., Mulitza, S., Pätzold, J., and Wefer, G.: Stable isotope data of sediment core GeoB1503-1, PANGAEA, [data set],
       https://doi.org/10.1594/PANGAEA.223482, 1997a.

Dürkoop, A., Hale, W., Mulitza, S., Pätzold, J., and Wefer, G.: Stable isotope data of sediment core GeoB2125-1, PANGAEA, [data set],
       https://doi.org/10.1594/PANGAEA.223488, 1997b.

Dürkoop, A., Hale, W., Mulitza, S., Pätzold, J., and Wefer, G.: Stable isotope data of sediment core GeoB2202-4, PANGAEA, [data set],
805   https://doi.org/10.1594/PANGAEA.223489, 1997c.

Dyez, K. A., Zahn, R., and Hall, I. R.: Multicentennial Agulhas leakage variability and links to North Atlantic climate during the past 80,000
       years, Paleoceanography, 29, 1238–1248, https://doi.org/10.1002/2014PA002698, 2014.

Freimüller, J.: Eine hochauflösende planktische Isotopenaufzeichnung des Heinrich Event 1 im tropischen Südamerika, Bachelor thesis,
       Fachbereich Geowissenschaften, Universität Bremen, 2013.

810   Ge, H., Li, Q., and Cheng, X.: Late Quaternary high resolution monsoon records in planktonic stable isotopes from northern South China
       Sea(in Chinese), Earth Sci: J China Uni Geosci, 35, 515–525, https://doi.org/10.3799/dqkx.2010.000, 2010.

Gemmeke, B.: Spätquartäre Variationen der Sauerstoffisotopen-Zusammensetzung des Oberflächenwassers im östlichen tropischen Nordat-
       lantik, Bachelor thesis, Fachbereich Geowissenschaften, Universität Bremen, 2010.

Gibbons, F. T., Oppo, D. W., Mohtadi, M., Rosenthal, Y., Cheng, J., Liu, Z., and Linsley, B. K.: Deglacial δ^{18}O and hydrologic variability
815   in the tropical Pacific and Indian Oceans, Earth and Planetary Science Letters, 387, 240–251, https://doi.org/10.1016/j.epsl.2013.11.032,
       2014.

Gingele, F., De Deckker, P., and Norman, M.: Late Pleistocene and Holocene climate of SE Australia reconstructed from
       dust and river loads deposited offshore the River Murray Mouth, Earth and Planetary Science Letters, 255, 257–272,
       https://doi.org/10.1016/j.epsl.2006.12.019, 2007.

820   Govil, P. and Divakar Naidu, P.: Variations of Indian monsoon precipitation during the last 32 kyr reflected in the surface hydrography of the
       Western Bay of Bengal, Quaternary Science Reviews, 30, 3871–3879, https://doi.org/10.1016/j.quascirev.2011.10.004, 2011.

Hale, W. and Pflaumann, U.: Stable isotopes on Globigerinoides ruber in sediment core GeoB2109-1, PANGAEA, [data set],
       https://doi.org/10.1594/PANGAEA.140002, 1999.

Holbourn, A., Kuhnt, W., Kawamura, H., Jian, Z., Grootes, P., Erlenkeuser, H., and Xu, J.: Orbitally paced paleoproductivity
825   variations in the Timor Sea and Indonesian Throughflow variability during the last 460 kyr, Paleoceanography, 20, PA3002,
       https://doi.org/10.1029/2004PA001094, 2005.

Hou, A., Bahr, A., Raddatz, J., Voigt, S., Greule, M., Albuquerque, A. L., Chiessi, C. M., and Friedrich, O.: Insolation and Greenhouse
       Gas Forcing of the South American Monsoon System Across Three Glacial-Interglacial Cycles, Geophysical Research Letters, 47,
       e2020GL087 948, https://doi.org/10.1029/2020GL087948, 2020.

830   Ivanova, E., Schiebel, R., Singh, A. D., Schmiedl, G., Niebler, H.-S., and Hemleben, C.: Primary production in the Arabian Sea during the last
       135 000 years, Palaeogeography, Palaeoclimatology, Palaeoecology, 197, 61–82, https://doi.org/10.1016/S0031-0182(03)00386-9, 2003.

Johnstone, H. J. H., Kiefer, T., Elderfield, H., and Schulz, M.: Calcite saturation, foraminiferal test mass, and Mg/Ca-based temperatures dissolution corrected using XDX—A 150 ka record from the western Indian Ocean, Geochemistry, Geophysics, Geosystems, 15, 781–797, https://doi.org/10.1002/2013GC004994, 2014.

835 Keigwin, L. D.: Radiocarbon and stable isotope constraints on Last Glacial Maximum and Younger Dryas ventilation in the western North Atlantic, Paleoceanography, 19, PA4012, doi: 10.1029/2004PA001 029, 2004.

Kemle-von Mücke, S.: Oberflächenwasserstruktur und -zirkulation des Südostatlantiks im Spätquartär, PhD thesis, Berichte aus dem Fachbereich Geowissenschaften der Universität Bremen, 55, 151 pp., 1994.

Knaack, J.: Eine neue Transferfunktion zur Rekonstruktion der Paläoproduktivität aus Gemeinschaften mariner Diatomeen, PhD thesis,
840 Geologisch-Paläontologisches Institut und Museum, Christian-Albrechts-Universität Kiel, 119 pp., 1997.

Knaack, J.-J. and Sarnthein, M.: Stable isotopes of foraminifera of ODP Hole 108-658C, PANGAEA, [data set], https://doi.org/10.1594/PANGAEA.227736, 2005.

Kohn, M., Steinke, S., Baumann, K.-H., Donner, B., Meggers, H., and Zonneveld, K. A.: Stable oxygen isotopes from the calcareous-walled dinoflagellate Thoracosphaera heimii as a proxy for changes in mixed layer temperatures off NW Africa during the last 45,000yr,
845 Palaeogeography, Palaeoclimatology, Palaeoecology, 302, 311–322, https://doi.org/10.1016/j.palaeo.2011.01.019, 2011.

Koutavas, A. and Lynch-Stieglitz, J.: Glacial-interglacial dynamics of the eastern equatorial Pacific cold tongue-Intertropical Convergence Zone system reconstructed from oxygen isotope records, Paleoceanography, 18, 1089, https://doi.org/10.1029/2003PA000894, 2003.

Leech, P. J., Lynch-Stieglitz, J., and Zhang, R.: Western Pacific thermocline structure and the Pacific marine Intertropical Convergence Zone during the Last Glacial Maximum, Earth and Planetary Science Letters, 363, 133 – 143, https://doi.org/10.1016/j.epsl.2012.12.026, 2013.

850 Li, L., Wang, H., Li, J., Zhao, M., and Wang, P.: Changes in sea surface temperature in western South China Sea over the past 450 ka, Chinese Science Bulletin, 54, 3335–3343, https://doi.org/10.1007/s11434-009-0083-9, 2009.

Li, Q., Zheng, F., Chen, M., Xiang, R., Qiao, P., Shao, L., and Cheng, X.: Glacial Paleoceanography off the Mouth of the Mekong River, Southern South China Sea, During the last 500 ka, Quaternary Research, 73, 563–572, https://doi.org/10.1016/j.yqres.2010.03.003, 2010.

Linsley, B. K.: Oxygen-isotope record of sea level and climate variations in the Sulu Sea over the past 150,000 years, Nature, 380, 234–237,
855 https://doi.org/10.1038/380234a0, 1996.

Lo, L., Chang, S.-P., Wei, K.-Y., Lee, S.-Y., Ou, T.-H., Chen, Y.-C., Chuang, C.-K., Mii, H.-S., Burr, G. S., Chen, M.-T., Tung, Y.-H., Tsai, M.-C., Hodell, D. A., and Shen, C.-C.: Nonlinear climatic sensitivity to greenhouse gases over past 4 glacial/interglacial cycles, Scientific Reports, 7, 4626, https://doi.org/10.1038/s41598-017-04031-x, 2017.

Lynch-Stieglitz, J., Polissar, P. J., Jacobel, A. W., Hovan, S. A., Pockalny, R. A., Lyle, M., Murray, R. W., Ravelo, A. C., Bova,
860 S. C., Dunlea, A. G., Ford, H. L., Hertzberg, J. E., Wertman, C. A., Maloney, A. E., Shackford, J. K., Wejnert, K., and Xie, R. C.: Glacial-interglacial changes in central tropical Pacific surface seawater property gradients, Paleoceanography, 30, 423–438, https://doi.org/10.1002/2014PA002746, 2015.

Meinecke, G.: Spätquartäre Oberflächenwassertemperaturen im östlichen äquatorialen Atlantik, PhD thesis, Berichte aus dem Fachbereich Geowissenschaften der Universität Bremen, 29, 181 pp., 1992.

865 Michael, S., Helmut, E., von Grafenstein, R., and Schroeder, C.: Stable-isotope stratigraphy for the last 750,000 years; Meteor core 13519 from the eastern equatorial Atlantic, Meteor-Forschungsergebnisse Reihe C Geologie und Geophysik, C38, 9–24, 1984.

Mohtadi, M., Lückge, A., Steinke, S., Groeneveld, J., Hebbeln, D., and Westphal, N.: Late Pleistocene surface and thermocline conditions of the eastern tropical Indian Ocean, Quaternary Science Reviews, 29, 887–896, https://doi.org/10.1016/j.quascirev.2009.12.006, 2010a.

Mohtadi, M., Steinke, S., Lückge, A., Groeneveld, J., and Hathorne, E. C.: Glacial to Holocene surface hydrography of the tropical eastern Indian Ocean, Earth and Planetary Science Letters, 292, 89–97, https://doi.org/10.1016/j.epsl.2010.01.024, 2010b.

Mohtadi, M., Oppo, D. W., Steinke, S., Stuut, J.-B. W., De Pol-Holz, R., Hebbeln, D., and Luckge, A.: Glacial to Holocene swings of the Australian-Indonesian monsoon, Nature Geoscience, 4, 540–544, https://doi.org/10.1038/ngeo1209, 2011.

Mohtadi, M., Prange, M., Oppo, D. W., De Pol-Holz, R., Merkel, U., Zhang, X., Steinke, S., and Luckge, A.: North Atlantic forcing of tropical Indian Ocean climate, Nature, 509, 76–80, https://doi.org/10.1038/nature13196, 2014.

Monteagudo, M. M., Lynch-Stieglitz, J., Marchitto, T. M., and Schmidt, M. W.: Central Equatorial Pacific Cooling During the Last Glacial Maximum, Geophysical Research Letters, 48, e2020GL088 592, https://doi.org/10.1029/2020GL088592, 2021.

Moros, M., De Deckker, P., Jansen, E., Perner, K., and Telford, R. J.: Holocene climate variability in the Southern Ocean recorded in a deep-sea sediment core off South Australia, Quaternary Science Reviews, 28, 1932–1940, https://doi.org/10.1016/j.quascirev.2009.04.007, 2009.

Mulitza, S.: Spätquartäre Variationen der oberflächennahen Hydrographie im westlichen äquatorialen Atlantik., PhD thesis, Berichte aus dem Fachbereich Geowissenschaften der Universität Bremen, 57, 95 pp., 1994.

Mulitza, S.: Globigerinoides ruber (white) isotopes of sediment core GeoB2109-1, PANGAEA, [data set], https://doi.org/10.1594/PANGAEA.713179, 2009.

Mulitza, S., Arz, H., von Mücke, S. K., Moss, C., Niebler, H.-S., Pätzold, J., and Segl, M.: The South Atlantic Carbon Isotope record of planktic foraminifera, in: Use of proxies in Paleoceanography: Examples from the South Atlantic, edited by Fischer, G. and Wefer, G., pp. 427–445, Springer Verlag, Berlin, Heidelberg, Germany, https://doi.org/10.1007/978-3-642-58646-0_17, 1999.

Mulitza, S., Bickert, T., Bostock, H. C., Chiessi, C. M., Donner, B., Govin, A., Harada, N., Huang, E., Johnstone, H., Kuhnert, H., Langner, M., Lamy, F., Lembke-Jene, L., Lisiecki, L., Lynch-Stieglitz, J., Max, L., Mohtadi, M., Mollenhauer, G., Muglia, J., Nürnberg, D., Paul, A., Rühlemann, C., Repschläger, J., Saraswat, R., Schmittner, A., Sikes, E. L., Spielhagen, R. F., and Tiedemann, R.: World Atlas of late Quaternary Foraminiferal Oxygen and Carbon Isotope Ratios, Earth System Science Data, 14, 2553–2611, https://doi.org/10.5194/essd-14-2553-2022, 2022.

Naik, S. S. and Naidu, P. D.: Carbonate preservation during the 'mystery interval' in the northern Indian Ocean, Geochemical Journal, 50, 357–362, https://doi.org/10.2343/geochemj.2.0420, 2016.

Parker, A. O., Schmidt, M. W., Jobe, Z. R., and Slowey, N. C.: A new perspective on West African hydroclimate during the last deglaciation, Earth and Planetary Science Letters, 449, 79–88, https://doi.org/10.1016/j.epsl.2016.05.038, 2016.

Patrick, A. and Thunell, R. C.: Tropical Pacific sea surface temperatures and upper water column thermal structure during the Last Glacial Maximum, Paleoceanography, 12, 649–657, https://doi.org/10.1029/97PA01553, 1997.

Paul, A., Reimer, J. J. G., Fürstenau, J., Kinkel, H., and Betzler, C.: Relationship between Late Pleistocene sea-level variations, carbonate platform morphology and aragonite production (Maldives, Indian Ocean), Sedimentology, 59, 1640–1658, https://doi.org/10.1111/j.1365-3091.2011.01319.x, 2012.

Portilho-Ramos, R. C., Cruz, A. P. S., Barbosa, C. F., Rathburn, A. E., Mulitza, S., Venancio, I. M., Schwenk, T., Rühlemann, C., Vidal, L., Chiessi, C. M., and Silveira, C. S.: Methane release from the southern Brazilian margin during the last glacial, Scientific Reports, 8, 5948, https://doi.org/10.1038/s41598-018-24420-0, 2018.

Raza, T., Ahmad, S. M., Sahoo, M., Banerjee, B., Bal, I., Dash, S., Suseela, G., and Mukherjee, I.: Hydrographic changes in the southern Bay of Bengal during the last ∼65,000 y inferred from carbon and oxygen isotopes of foraminiferal fossil shells, Quaternary International, 333, 77–85, https://doi.org/10.1016/j.quaint.2014.02.010, 2014.

Richter, T.: Sedimentary fluxes at the Mid-Atlantic Ridge: sediment sources, accumulation rates, and geochemical characterisation, PhD thesis, GEOMAR-Report, 73, GEOMAR Research Center for Marine Geosciences, Christian-Albrechts-Universität in Kiel, 173 pp., Kiel, https://doi.org/10.3289/GEOMAR_REP_73_1998, 1998.

910 Romahn, S.: Western Indian Ocean circulation and climate variability on different time scales: a study based on stable oxygen and carbon isotopes, benthic foraminiferal assemblages and Mg/Ca paleothermometry, PhD thesis, Fachbereich Geowissenschaften, Universität Bremen, 95 pp., 2014.

Romahn, S., Mackensen, A., Groeneveld, J., and Pätzold, J.: Deglacial intermediate water reorganization: new evidence from the Indian Ocean, Climate of the Past, 10, 293–303, https://doi.org/10.5194/cp-10-293-2014, 2014.

915 Rühlemann, C., Frank, M., Hale, W., Mangini, A., Mulitza, S., Müller, P., and Wefer, G.: Late Quaternary productivity changes in the western equatorial Atlantic: Evidence from 230Th-normalized carbonate and organic carbon accumulation rates, Marine Geology, 135, 127–152, https://doi.org/10.1016/S0025-3227(96)00048-5, 1996.

Sarnthein, M., Winn, K., Duplessy, J.-C., and Fontugne, M. R.: Global variations of surface ocean productivity in low and mid latitudes: Influence on CO_2 reservoirs of the deep ocean and atmosphere during the last 21,000 years, Paleoceanography, 3, 361–399,
920 https://doi.org/10.1029/PA003i003p00361, 1988.

Sarnthein, M., Winn, K., Jung, S. J. A., Duplessy, J. C., Labeyrie, L., Erlenkeuser, H., and Ganssen, G.: Changes in East Atlantic deepwater circulation over the last 30,000 years: eight time slice reconstruction, Paleoceanography, 99, 209–268, https://doi.org/10.1029/93PA03301, 1994.

Schefuß, E., Schouten, S., and Schneider, R. R.: Climatic controls on central African hydrology during the past 20,000 years, Nature, 437,
925 1003–1006, https://doi.org/10.1038/nature03945, 2005.

Schneider, R.: Spätquartäre Produktivitätsänderungen im östlichen Angola-Becken: Reaktion auf Variationen im Passat-Monsun-Windsystem und in der Advektion des Benguela-Küstenstroms, PhD thesis, Berichte aus dem Fachbereich Geowissenschaften der Universität Bremen, 21, 198 pp., Bremen, 1991.

Shackleton, N., Le, J., Mix, A., and Hall, M.: Carbon isotope records from pacific surface waters and atmospheric carbon dioxide, Quaternary
930 Science Reviews, 11, 387–400, https://doi.org/10.1016/0277-3791(92)90021-Y, 1992.

Sirocko, F.: Zur Akkumulation von Staubsedimenten im nördlichen Indischen Ozean, Anzeiger der Klimageschichte Arabiens und Indiens: = Accumulation of eolian sediments in the northern Indian Ocean, record of the climatic history of Arabia and India, PhD thesis, Geolog.-Paläontolog. Inst. u. Museum, Christian-Albrechts-Univity, Kiel, Berichte. 27, 185 pp., 1989.

Sirocko, F., Garbe-Schönberg, D., and Devey, C.: Processes controlling trace element geochemistry of Arabian Sea sediments during the last
935 25,000 years, Global and Planetary Change, 26, 217–303, https://doi.org/10.1016/S0921-8181(00)00046-1, 2000.

Slowey, N. C.: The modern and glacial thermoclines along the Bahama Banks, PhD thesis, Massachusetts Institute of Technology and Woods Hole Oceanographic Institution, 1990.

Slowey, N. C. and Curry, W. B.: Enhanced ventilation of the North Atlantic subtropical gyre thermocline during the last glaciation, Nature, 358, 665–668, https://doi.org/10.1038/358665a0, 1992.

940 Spero, H. J., Mielke, K. M., Kalve, E. M., Lea, D. W., and Pak, D. K.: Multispecies approach to reconstructing eastern equatorial Pacific thermocline hydrography during the past 360 ky, Paleoceanography, 18, 1022, https://doi.org/10.1029/2002PA000814, 2003.

Stott, L., Poulsen, C., Lund, S., and Thunell, R.: Super ENSO and Global Climate Oscillations at Millennial Time Scales, Science, 297, 222–226, https://doi.org/10.1126/science.1071627, 2002.

Stott, L., Timmermann, A., and Thunell, R.: Southern hemisphere and deep-sea warming led deglacial atmospheric CO_2 rise and tropical
945   warming, Science, 318, 435–438, doi: 10.1126/science.1143 791, 2007.

Tian, J., Huang, E., and Pak, D. K.: East Asian winter monsoon variability over the last glacial cycle: Insights from a latitudinal
       sea-surface temperature gradient across the South China Sea, Palaeogeography, Palaeoclimatology, Palaeoecology, 292, 319–324,
       https://doi.org/10.1016/j.palaeo.2010.04.005, 2010.

Tierney, J. E., deMenocal, P. B., and Zander, P. D.: A climatic context for the out-of-Africa migration, Geology, 45, 1023–1026,
950   https://doi.org/10.1130/G39457.1, 2017.

Toledo, F. A., Costa, K. B., and Pivel, M. A.: Salinity changes in the western tropical South Atlantic during the last 30 kyr, Global and
       Planetary Change, 57, 383–395, https://doi.org/10.1016/j.gloplacha.2007.01.001, 2007.

Vahlenkamp, M.: The Anatomy of Heinrich Event 1 — A Multiproxy Study of Centennial to Millennial Scale Climate Change off Brazil,
       Master thesis, Fachbereich Geowissenschaften, Universität Bremen, 2013.

955   Venancio, I. M., Mulitza, S., Govin, A., Santos, T. P., Lessa, D. O., Albuquerque, A. L. S., Chiessi, C. M., Tiedemann, R.,
       Vahlenkamp, M., Bickert, T., and Schulz, M.: Millennial- to Orbital-Scale Responses of Western Equatorial Atlantic Thermocline
       Depth to Changes in the Trade Wind System Since the Last Interglacial, Paleoceanography and Paleoclimatology, 33, 1490–1507,
       https://doi.org/10.1029/2018PA003437, 2018.

von Rad, U., Schulz, H., Riech, V., den Dulk, M., Berner, U., and Sirocko, F.: Multiple monsoon-controlled breakdown of oxygen-minimum
960   conditions during the past 30,000 years documented in laminated sediments off Pakistan, Palaeogeography, Palaeoclimatology, Palaeoe-
       cology, 152, 129–161, https://doi.org/10.1016/S0031-0182(99)00042-5, 1999.

Wang, L., Sarnthein, M., Erlenkeuser, H., Grimalt, J., Grootes, P., Heilig, S., Ivanova, E., Kienast, M., Pelejero, C., and Pflaumann, U.: East
       Asian monsoon climate during the Late Pleistocene: high-resolution sediment records from the South China Sea, Marine Geology, 156,
       245–284, https://doi.org/10.1016/S0025-3227(98)00182-0, 1999.

965   Wang, P., Li, Q., Tian, J., He, J., Jian, Z., Ma, W., and Dang, H.: Monsoon influence on planktic δ^{18}O records from the South China Sea,
       Quaternary Science Reviews, 142, 26–39, https://doi.org/10.1016/j.quascirev.2016.04.009, 2016.

Wang, Y. V., Leduc, G., Regenberg, M., Andersen, N., Larsen, T., Blanz, T., and Schneider, R. R.: Northern and southern hemisphere
       controls on seasonal sea surface temperatures in the Indian Ocean during the last deglaciation, Paleoceanography, 28, 619–632,
       https://doi.org/10.1002/palo.20053, 2013.

970   Wefer, G., Berger, W. H., Bickert, T., Donner, B., Fischer, G., von Mücke, S. K., Meinecke, G., Müller, P. J., Mulitza, S., Niebler, H.-
       S., Pätzold, J., Schmidt, H., Schneider, R. R., and Segl, M.: Late Quaternary Surface Circulation of the South Atlantic: The Stable
       Isotope Record and Implications for Heat Transport and Productivity, pp. 461–502, Springer Berlin Heidelberg, Berlin, Heidelberg,
       https://doi.org/10.1007/978-3-642-80353-6_25, 1996.

Winn, K.: Density, carbon and stable isotope ratios of foraminifera from sediment core SO35-272, PANGAEA, [data set], in: Winn, Kyaw;
975   Werner, Friedrich; Erlenkeuser, Helmut (2013): Age model and stable isotope ratios of sediment cores from the South China Sea. PAN-
       GAEA, https://doi.org/10.1594/PANGAEA.807876, 2013.

Zahn-Knoll, R.: Spätquatäre Entwicklung von Küstenauftrieb und Tiefenwasserzirkulation im Nordost-Atlantik. Rekonstruktion anhand
       stabiler Isotope kalkschaliger Foraminiferen, PhD thesis, Christian-Albrechts-Universität zu Kiel, 111 pp., 1986.

Zimmermann, R.: Spätquartäre Geschichte der Oberflächenstratifizierung im Golf von Guinea anhand des Schwerelotkernes GeoB 4905-4,
980   Bachelor thesis, Fachbereich Geowissenschaften, Universität Bremen, 2013.